TU Delft

Bachelor Thesis

Linear analysis of a natural circulation driven supercritical water loop

D J van der Ham
4285816

supervised by
Dr. Ir. M. Rohde

July 3, 2016

Nomenclature

Symbol	Units	Description
A	m^2	Length
A_w	m^2	Wall-cross-sectional area
C_i	m^{-3}	Precursor concentration
D_H	m	Hydraulic diameter
E_f	J	Energy per fission event
H	J kg^{-1}	Specific enthalpy
K	$-$	Pressure loss coefficient
L	m	Length (without subscript: total core length)
M	g mol^{-1}	Molar mass
N	m^{-3}	Number density
N_A	mol^{-1}	Avogadro constant
Pin	m	Perimeter
Q	J s^{-1}	Core heating power
Qw	J s^{-1}	Fuel-to-wall heat flow
R		Reactivity
T	K	Temperature
V	m^3	Volume
V_f	m^3	Fuel volume
W	kg s^{-1}	Mass flow rate
c_p	J kg^{-1} K^{-1}	Fluid specific heat
$c_{p,w}$	J kg^{-1} K^{-1}	Wall material specific heat
f		Darcy friction factor
g	m s^{-2}	Gravitational acceleration
h	J kg^{-1}	Specific enthalpy
n	m^{-3}	Neutron concentration
p	N m^{-2}	Pressure
t	s	Time
v_n	m s^{-1}	Neutron velocity
Λ	s	Mean generation time
Σ_f	m^{-1}	Macroscopic neutronic cross-section for thermal fission
α_r	m^3 kg^{-1}	Density reactivity feedback coefficient
β		Delayed neutron fraction
ϵ		Enrichment
θ	K	Temprature pertubation
λ		Eigenvalue
λ_f	J s^{-1} m^{-1} K^{-1}	Fluid thermal conductivity
λ_i	s^{-1}	Precursor decay constant

λ_w	J s^{-1} m^{-1} K^{-1}	Wall thermal conductivity
μ	N s m^{-2}	Dynamic viscosity
ρ	kg m^{-3}	Density
ρ_w	kg $m^{/3}$	Wall material density
σ_f	m^{-3}	Microscopic neutronic cross-section for thermal fission
τ	s	Fuel heat transfer time constant

Dimensionless numbers

N_{fr}	Froude number
N_{sub}	Subcooling number
$N_{\Delta h}$	Pseudo phase change number
Nu	Nusselt number

Subscripts	Value at:
0	Bottom core node
1	Top core node
B	Buffer vessel node
D	Downcomer node
F	Fuel node
R	Riser node
pc	Pseudo-critical point
w	Wall node (low heating model)
$w, 0$	Top wall node (high heating model
$w, 1$	Top wall node (high heating model)

Other

$\overline{X}$		Steady state variable
$\underline{X}$		Dimensionless variable
$\check{x}$		Pertubation on variable
$\widehat{Nu}$	$W^{0.66}$ $m^{-0.66}$ $K^{-0.66}$	Adjusted Nusselt number

Commom abbreviations

BWR	Boiling Water Reactor
DR	Decay Ratio
DWO	Density Wave Oscillations
GIF	Feneration IV International Forum
HPLWR	High Performance Light Water Reactor
SCWR	Supercritical Water-cooled Reactor

Abstract

The High Performance Light Water Reactor (HPLWR) is a European reactor based on the Generation IV Supercritical Water-cooled Reactor (SCWR) concept. This reactor is designed to be more environmentally friendly and more efficient. Furthermore, it can be designed to rely on natural circulation as its driving force, eliminating active pumps thus making it more safe. This does cause the reactor to be unstable under certain operating conditions. This thesis will use and extend an existing model to investigate and better understand these instabilities by looking at them under different parameters as well as by analyzing the frequency and time dependent behavior of the perturbations on the systems variables.

In this model the reactor is reduced to several nodes. Conservation balances are set up and linearized for all nodes. The remaining equations are written as a matrix equation, reducing the problem to an eigenvalue problem. The steady state solutions are found through an iterative process and the stability is determined for all operating conditions. The results can then be plotted on an instability map

Through a parametric study in which the hydraulic diameter and length of the riser were varied simultaneously, it was found that for a small hydraulic diameter increasing the length makes the system less stable. For a high hydraulic diameter, occurrence of instabilities associated with gravity increase, but those associated with friction decrease.

The resonance frequency was found to be almost constant on a line that passes through the origin of an instability plot. Using this result, a linear relationship was found between the resonance frequency and the dimensionless density and frequency of water the part of the core where its subcritical.

A time dependent solution for the problem was found. Using this solution friction proved to be a bigger factor in the perturbation of the solution than gravity for most operating conditions, particularly in the riser. The frequency of all perturbations for constant parameters was found to be the same for different perturbations.

Contents

1 Introduction

1.1 Background of Research

By the year 2050, human population is expected to have grown to ten billion individuals [7]. Combined with the ever increasing global average wealth means that the demand for energy will continue to increase for many years to come [11]. Since restraining that energy consumption leads to a lower standard of living and halts economic growth [11] and fossil fuels are considered a main contributor to global warming [7], the need for new energy sources continues to be high.

To meet these demands, the U.S. Department of Nuclear Energy, Science and Technology founded the Generation IV International Forum (GIF). The goal of this international organization is to carry out research and development needed to evaluate the next generation, or generation IV, nuclear energy systems [6]. To this end, GIF has selected six systems for further development. They are looking to deploy the first commercial generation IV reactors in about two decades.

One such system is the Supercritical Water-cooled Reactor (SCWR). This is the reactor that The Nuclear Energy and Radiation Applications section of Delft University of Technology (NERA) performs research in [12]. The SCWR utilizes a similar principle as the second and third generation reactors Boiling water reactor (BWR) and Pressurized water reactor (PWR), which right now are the two most common reactors [17]. All these reactors rely on water to both moderate the neutrons and act as a coolant. The difference is that the SCWR operates under much higher temperature and pressure, which bring the water above its supercritical point.

1.2 Supercritical Fluids

The equilibrium state of water is dependent on both the temperature and the pressure, as seen in the phase diagram in figure 1.1. There are various different states water can be in as a result of these two. The three colored lines are called change lines, as they indicate for which conditions water transition from one of the three most common states to another. These lines meet at the triplet point, where water can be in any of the three states.

The other interesting point marked in the diagram is the pseudo-critical point (dubbed critical point in figure 1.1. At the pseudo-critical point, the densities of vapor created by the increase in in temperature and the liquid water are identical. Water in this state is called supercritical. Thus any combination of temperature and pressure where both are equal or higher then their values at the pseudo-critical point makes the water supercritical. It can not be said that there is an actual phase change, but its properties do change quite drastically. The properties of water at the pseudo-critical point can be seen in table 1.1.

Table 1.1: Properties of water at the pseudo-critical point

Property	Value
T_{pc}	384.9 °C
p_{pc}	22.06 MPa
h_{ph}	$2.1529 * 10^6$ J/ kg
ρ_{pc}	316.81 kg/m^3
v_{ph}	$3.1564 * 10^{-3}$$m^3$/ kg
μ_{ph}	$4.2797 * 10^{-5}$ Pa∗s

Note that a SCWR generally maintains a constant pressure of 25 MPa [7], well above the critical pressure $p_c = 22.06$ MPa. The average temperature of the water

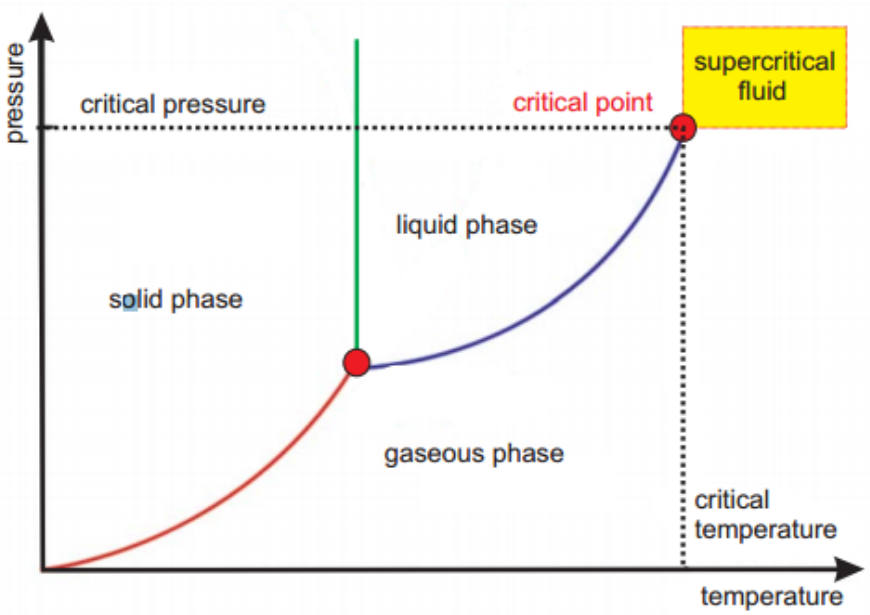

Figure 1.1: Phase diagram supercritical fluids [7]

in a SCWR is assumed to go from about 280 °C to 500 °C. Since the critical temperature of water in the reactorT_{pc} = 384.9 °C, in the reactor it always transitions from a liquid phase to a supercritical fluid (see figure 1.1).

This is mostly desirable because of the large variation of the specific heat capacity around the pseudo-critical point. Specific heat capacity, along with several other properties such as density and viscosity, shows highly non-linear temperature behaviour around the pseudo-critical point. As can be seen in figure 1.2, the specific heat capacity has a sharp and fairly high peak at $T = T_{pc}$. This allows significantly more heat to be stored in the water with only small temperature changes.

1.3 High Performance Light Water Reactor

The basic workings of a SCWR can be seen in figure 1.3. Liquid water enters the core, where nuclear reactions heat it to be supercritical. The supercritical water then flows through a turbine, where the heat is converted to electricity through a generator. Then the water enters a condenser, where it is cooled back to the inlet temperature, after which it can enter the core again.

SCWRs have a multitude of advantages over current reactor [5]. These include a higher thermal efficiency of 45% (vs 34-36% for current reactors). Some SCWR designs also make the inclusion of a pump obsolete. Another property of supercritical water is that its density drops very rapidly with temperature around the pseudo-critical point, meaning there is a large density difference in the reactor. This is sufficient to provide a driving force for the loop. Due to the heat capacity peak, less water is needed to cool the core, making smaller reactors more viable.

One of the reactors that utilizes Supercritical water is the High Performance Light Water Reactor (HPLWR), a European version of the SCWR. The HPLWR is what this report will analyze.

HPLWR reactors mostly set themselves apart from other SCWRs through their core design, which can be seen in figure 1.4. The core of a HPLWR is a three-pass core design, meaning it consists of three heating sections with mixing chambers between them. The water is first brought to a uniform 310 °C

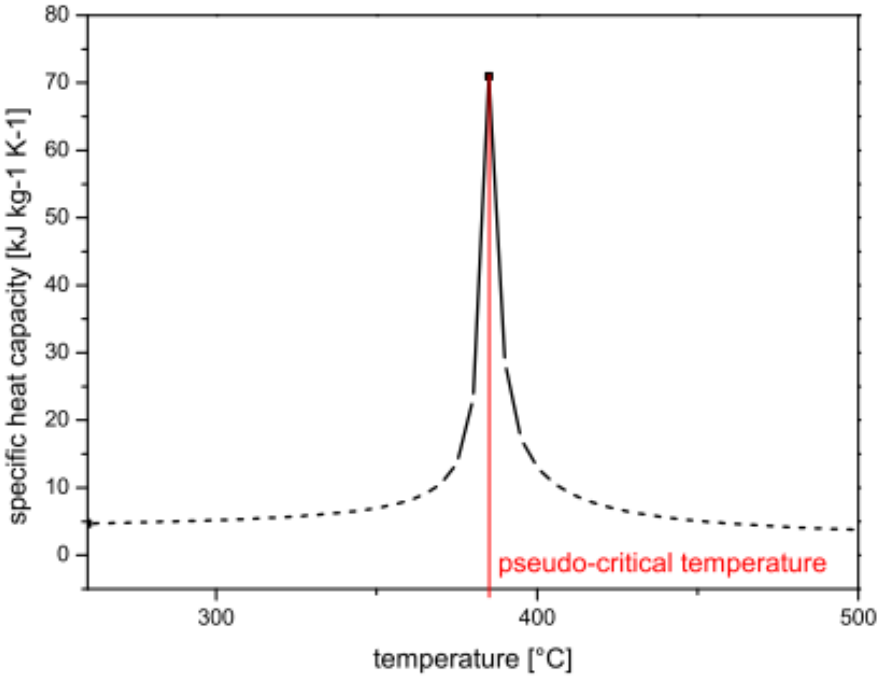

Figure 1.2: Specific heat capacity vs temperature for all temperatures found in SCWR at 25 MPa. The specific heat capacity peaks at the pseudo-critical point at T_{pc}=384.9 °C [7]

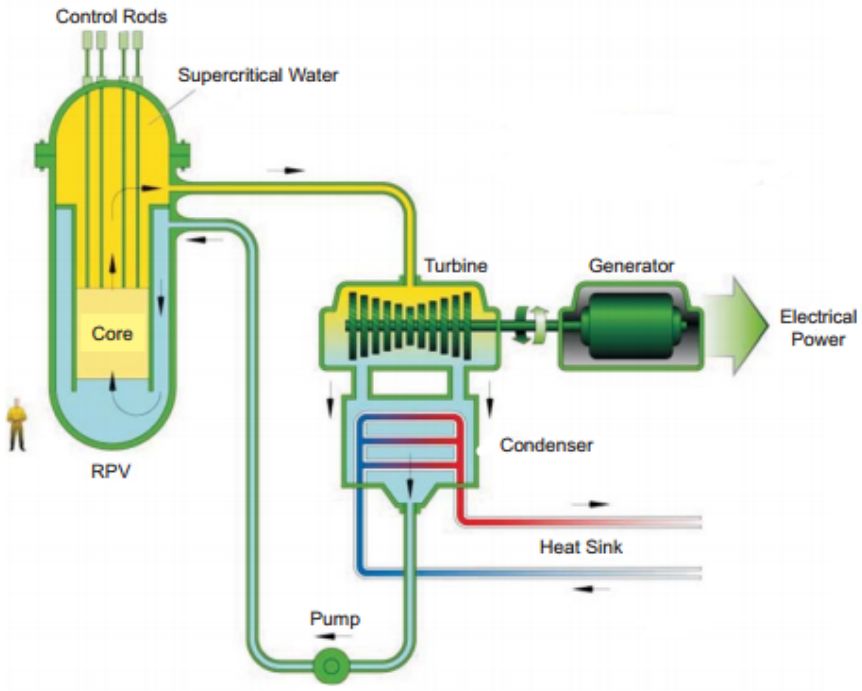

Figure 1.3: Simplified overview of a SCWR. [7]

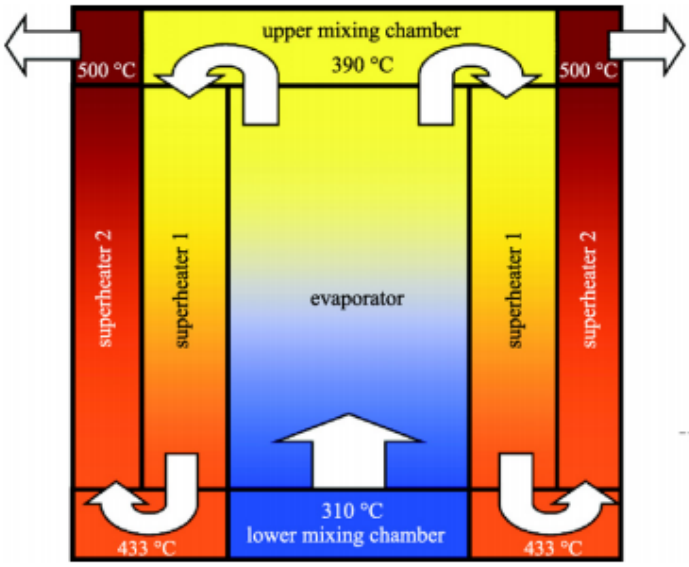

Figure 1.4: Concept of the core of a HPLWR [3]

and passes through the evaporator, which heats it to an average temperature of 390 °C. In the upper mixing chamber the water temperature is made uniform. It then flows through the first superheater, another mixer and another heater, bringing the final temperature to the 500 °C mentioned earlier. This leads to the density of the water to decrease from approximately 780 kg/m^3 to a mere 90 kg/m^3, providing a significant driving force for the water to flow [7].

This report will analyze a reactor where the force provided by the density difference throughout the loop is the only driving force, meaning it exclusively relies on natural convection. To enhance the flow, a riser is placed on top of the core, increasing gravitational pressure drop. Much to the same effect, a downcomer is added after the water is cooled down.

In pump driven reactors, technical failures or natural disasters may cause a power outage, preventing the pumps from working and thereby eliminating the moderation. The elimination of pumps thus decreases the risk of such events influencing the reactor, making it more safe in emergency situations.

1.4 Instabilities in the reactor

In order to be a viable working reactor, a system needs to be stable. This is the case for systems where a small perturbation from its steady state operating variables trigger a negative feedback loop, causing the system to return to said steady state. In talking about stability it is convenient to consider the decay ratio, which is defined as the ratio between two consecutive peaks. If a system responds to a perturbation with an oscillation with a decay ratio larger then one, every peak has a larger amplitude then the previous one. A decay ratio of larger then one thus means an unstable system, while a decay ratio smaller then one makes a system stable. This is visualized in figure 1.5. The system of the left graph has a small decay ratio, therefore returning to its steady state value. The right system has a larger decay ratio, making it oscillate with an ever increasing amplitude. Since the HPLWR relies on water as a moderator, instabilities in its properties greatly decrease the reactors safety and should thus be avoided.

Two types of instabilities are present in natural circulation driven BWRs [16]. Both of them are caused by local density differences and are known as Density Wave Oscillations (DWO). Specifically, type-I and type-II DWO's are present in BWRs. Type-I and type-II differ in how they are caused.

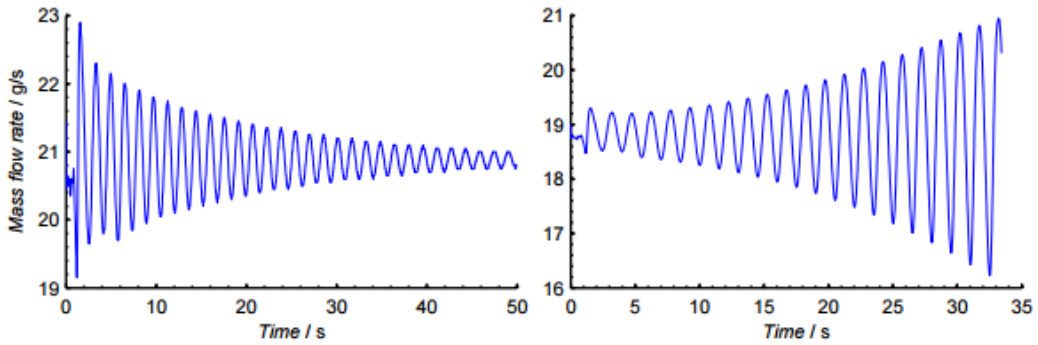

Figure 1.5: Example of reaction on permutation by a stable (left) and an unstable (right) system. [15]

Type-I DWO instabilities are associated with gravitational pressure drops and oscillates with low frequencies. Type-II on the other hand is caused by frictional pressure drops and oscillates at slightly higher frequencies (around 0.1-0.15 Hz [8]). In BWRs the water undergoes a phase change from liquid to vapor, while SCWRs are considered single phase. However, the density behavior of water around the pseudo-critical point is similar to its behavior around the boiling point, so the same types of instabilities are assumed to be present in the HPLWR.

Another type of instability that is often considered in two-phase flows is the Ledinegg instability. However, this report will focus on the two DWO instabilities discussed above as they are far more prevalent.

1.5 Previous research

Stability in natural circulation driven loops have been analyzed extensively by NERA [10][16]. An experimental setup named DeLight - short for Delft Light Water Reactor Facility - was built at TU Delft for this exact purpose [1]. Spoelstra and Schenderling performed numerical research on the setup, but their results varied from those of the experiment [14]. Note that Schenderling improved upon Spoelstra's model by taking into account the thermal inertia, causing his results to agree with the experiment more then Spoelstra's (see figure 1.6).

The stability of the HPLWR core was investigated by Ortega Gómez [7]. Here it was found that under forced circulation there were no Ledinegg instabilities and no pressure drop oscillations at steady state in the HPLWR. Also, DWO's were found to be the main type of instability present in the reactor.

Another numerical analysis was performed by Krijger [8]. A significant difference between Krijger's method and Spoelstra's is that Krijger divided the reactor into four or five nodes, depending on if the water reaches its pseudo-critical point. Inside these nodes, the variables are assumed to increase linearly. Krijger derived mass-, energy- and momentum balances for all these nodes and linearized these equations. The result was an eigenvalue problem he solved using a *Matlab* code. Krijger found that increasing the riser length had a destabilizing effect. These results do not agree with previous research done in BWRs by van Bragt [16], where increasing the riser length increased type I instabilities but decreased type II instabilities. Krijger also found that increasing the buffer volume improved the stability of the system.

Lippens [9] and Zonneveld [19] later improved on Krijger's model by adding and enhancing equations to include the thermal inertia and neutronic-thermal-hydraulic coupling respectively. Thermal inertia was found to improve the system's stability, while neutronic-thermal-hydraulic coupling decreased stability. De Vries [2] further expanded on this model by developing a method for finding the time-dependent behavior of system variables. The variables showed to have a decay ratio of larger for the expected conditions, but his results had some very peculiar and likely incorrect values, making

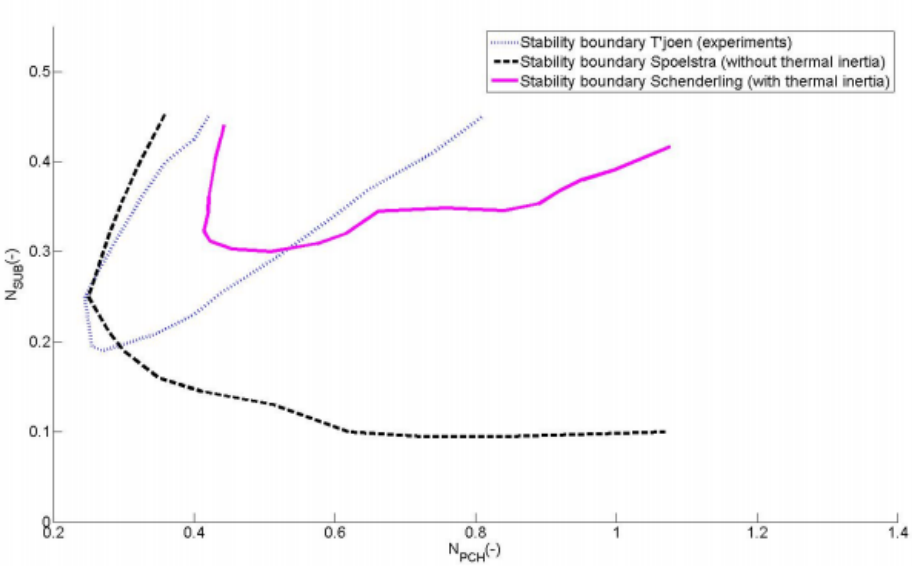

Figure 1.6: The experimental values found in DeLight with numerical results of Spoelstra's and Schenderling's numerical model. [14]

interpreting them meaningless.

1.6 Thesis outline

This theses will continue improving and expanding on Krijger's model. An improved parametric study will be performed, changing several parameters for different values of the riser length to investigate its (de)stabilizing effect. The frequency of the unstable regions will also be investigated. Finally, the time-dependency of the perturbed variables will be investigated.

The next chapter will cover the model used and the equations that are derived from it. This includes the structure of the loop and linearizing the equations that follow from it.

Chapter 3 describes how the equations chapter 2 ends on are converted to a matrix equation. It will then derive how the time-dependency of the perturbed variables can be determined. Chapter 4 will discuss how the conclusions of chapter 3 are implemented in a *Matlab* code in order to find all the eigenvalues and eigenvectors and all the steady state values of the system variables are found. Chapter 5 includes the parametric studies performed and introduces the analysis of the frequency in unstable regions of the system.

Chapter 6 presents the results obtained from the analysis presented in chapters 3 through 5. A brief interpretation of all the results is also included.

Finally, Chapter 7 gives the overall conclusions drawn from the analyses and discusses them, ending with recommendations for further research.

2 Physical model

This chapter will introduce the model the rest of the report uses to analyse the reactor. The equations that were derived from the assumptions made are also discussed.

2.1 HPLWR in nodes

In 2013, Krijger [8] adapted a model developed by Rohde, who again adapted a model used on boiling water reactors by Guido et al [4]. Purpose of said model was to determine the stability regions of a reactor. Lippens and Zonneveld took this model and expended on it. The visualization of the final model used by Zonneveld can be seen in figure 2.1.

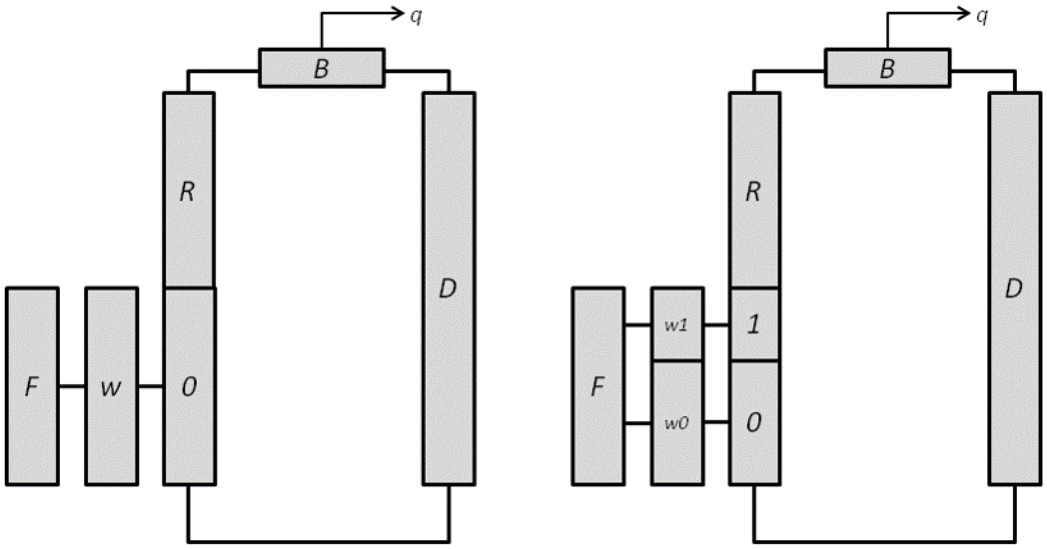

Figure 2.1: The HPLWR broken down into nodes. Water flows in the clockwise direction. Node labels are as follows: *F*: Fuel, *w0*: Wall node 0, *w1*: Wall node 1, *0*: Core node 0, *1*: Core node 1, *R*: Riser. *B*: Buffer, *D*: Downcomer. [19]

Subcritical water enters the core of the reactor at the bottom of node *0*. Here it absorbs heat, causing its temperature to rise. Depending on the operating conditions of the reactor, the temperature can increase enough to make the water supercritical, but this is not necessarily the case. If the water does reach its pseudo-critical point, the rest of the core (in which the water is supercritical) is dubbed node *1*. This is seen in the right loop of figure 2.1. If the water is not heated enough the entire core will be node *0*, as seen in the left loop in figure 2.1. These situations are called the high heating model and the low heating model respectively. Note that in the high heating model, the length of both node

0 and *1* are variables that depend on the operating conditions, while in the low heating model the length of node *0* is constant.

The riser and buffer nodes are the relatively straightforward parts of the reactor, as they are just tubes that the water flows through. The buffer node represents the turbine and heat exchanger together. It is where the water is cooled and the resulting heat is converted to electricity (depicted by the q in figure 2.1). The fuel and wall nodes do not interact with the water directly. The wall node is added to model the thermal inertia, while the fuel node accounts for heat transfer from the fuel to the wall.

2.2 Assumptions and simplifications

Several simplifications were made for this model. An important one involves the equation of state. The pressure of water is assumed to be a constant 25 MPa throughout the entire reactor, despite in reality there being local frictional and gravitational pressure drops. From this assumption we can say that the density of water is only dependent on its enthalpy. If water is subcritical, its density is assumed to decrease linearly with enthalpy. Once the enthalpy is large enough to make the water supercritical, the specific volume, which is the inverse of density, linearly increases with enthalpy. This leads to the formula seen in equation 2.1. To find the two constants C_1 and C_2 the equations is fitted through data from National Institute of Standards and Technology [13] (see figure 2.2.

$$v_i = \begin{cases} \frac{1}{\rho_{pc}+C_1(H_i-h_{pc})} & H_i < h_{pc} \\ v_{pc} + C_2(H_i - h_{pc}) & H_i \geq h_{pc} \end{cases} \tag{2.1}$$

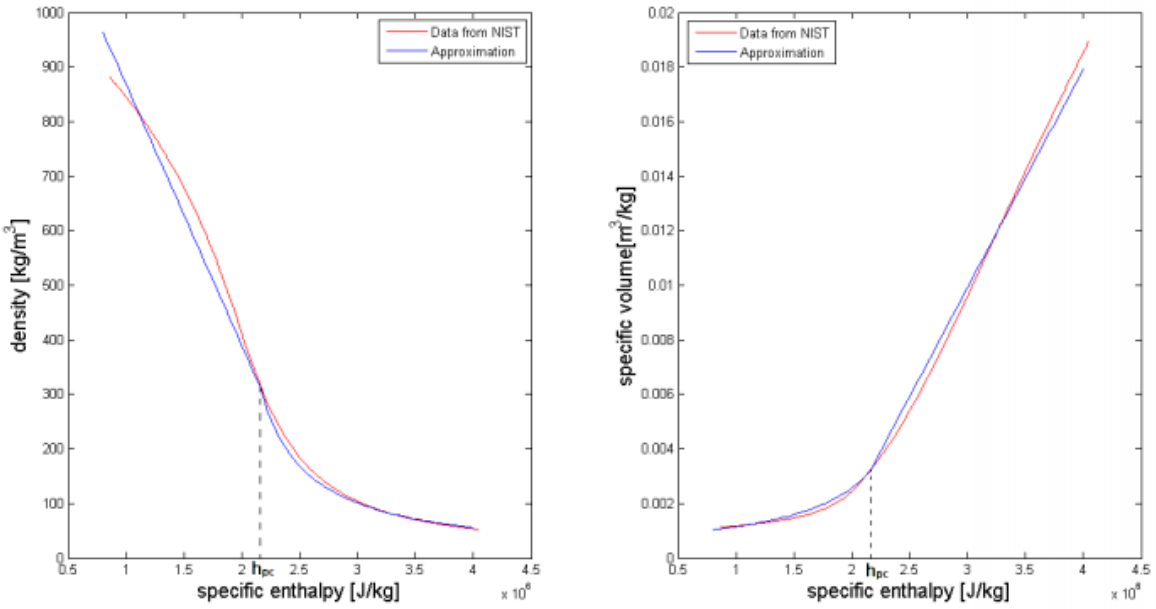

Figure 2.2: Equation 2.1 fitted through the data from NIST. [8]

The temperature is also approximated, using a quadratic function in both the sub- and supercritical region. This approximation and its slope need to be continuous around the pseudo-critical point. With the constants α_0 = -1.1∗10^{-10} KJ^{-2} and α_1 = -1.0∗10^{-10} KJ^{-2}, the following equation can be found:

$$T_i = \alpha_i(H_i - h_{pc})^2 + \frac{H_i - h_{pc}}{cp, pc} + T_{pc} \tag{2.2}$$

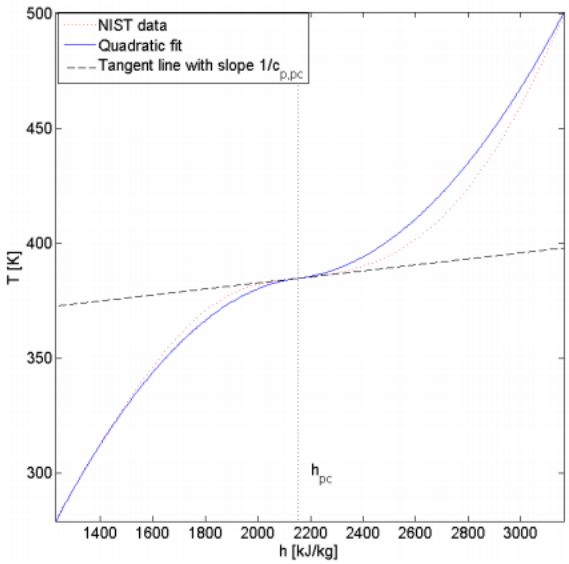

Figure 2.3: Equation 2.2 fitted through the data from NIST. [9]

Finally, the thermal conductivity is approximated with a linear function in the subcritical region and an exponential function in the high enthalpy region. Again, the approximation and slope are continuous at the pseudo-critical point.

$$\lambda_f = \begin{cases} -\beta_0 H_0 + \lambda_{f,b,0} & H_i < h_{pc} \\ \lambda_z e^{-\beta_1 H_1} + \lambda_{f,b,1} & H_i \geq h_{pc} \end{cases} \tag{2.3}$$

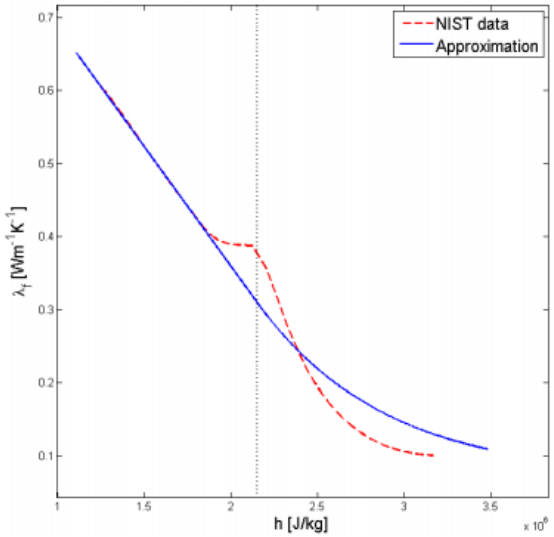

Figure 2.4: Equation 2.3 fitted through the data from NIST. [9]

The fit seen in figure 2.4 yields the following values [9]:

β_0 = -3.2711$*10^{-7}$
β_1 = 1.3694$*10^{-6}$ kgJ^{-1}
$\lambda_{f,b,0}$ = 1.0133 WM^{-1}K^{-1}
$\lambda_{f,b,1}$ = 7.0154$*10^{-2}$ WM $^{-1}$K^{-1}
λ_z = 4.5553 WM^{-1}K^{-1}

2.3 Balance equations

With the definitions in the previous section and the model introduced in section 2.1, transport equations can be derived for the mass, energy and momentum in every node. These equations can then be made dimensionless and linearized, leaving equations with only constants and perturbations.

These balances have all been derived by Krijger, Lippens and Zonneveld, so for this report most of them are merely included in appendix B. To illustrate how they are brought from their initial form to the linearized equations in the end, the high heating momentum balance will be used as an example. Note that opposed to the mass and energy balances, the momentum balance is integrated over the entire loop rather than over a single node. The initial high heating momentum balance is as follows:

$$\begin{aligned} A\frac{d}{dt}W_0L_0 + A\frac{d}{dt}W_1L_1 + AL_R\frac{d}{dt}W_R + \frac{d}{dt}V_BW_0 + AL_D\frac{d}{dt}W_0 = -(\frac{f_0L_0}{D_{H,0}} + K_0)\frac{W_0^2}{2\rho_0}... \\ ... - (\frac{f_1L_1}{D_{H,1}} + K_1)\frac{W_1^2}{2\rho_1} - (\frac{f_RL_R}{D_{H,r}} + K_r)\frac{W_R^2}{2\rho_R} - (\frac{f_DL_D}{D_{H,D}} + K_D)\frac{W_0^2}{2\rho_{in}}... \\ ... - A^2g\rho_0L_0 - A_2g\rho_1L_1 - A^2g\rho_RL_R - A^2g\rho_inL_D \end{aligned} \tag{2.4}$$

Note that L_0 and L_1 are both variables, as the length it takes water to reach its pseudo-critical point may vary. Yet when combined they must always total the length of the core, meaning L_0 can be substituted for $L - L_1$, with L being the total core length.

For the steady state solution for equation 2.4, the steady state mass flow needs to be calculated. In steady state, gravity and friction terms need to cancel each other perfectly, as there is no net force on the water. This means the following equation for the steady state mass flow is found.

$$\bar{W}_{HHM}^2 = gA^2\frac{\rho_{in}L_D - \hat{\rho}_0L - \hat{\rho}_RL_R}{(\frac{f_0L_0}{D_{H,0}} + K_0)\frac{1}{2\rho_0} + (\frac{f_1L_1}{D_{H,1}} + K_1)\frac{1}{2\rho_1} + (\frac{f_RL_R}{D_{H,r}} + K_r)\frac{1}{2\rho_R} + (\frac{f_DL_D}{D_{H,D}} + K_D)\frac{1}{2\rho_{in}}} \tag{2.5}$$

The variables in in equation 2.4 are then substituted for the dimensionless variables found in appendix A.

$$\begin{aligned} -\underline{W_0}\frac{d}{d\underline{t}}\underline{L_1} + (1 - \underline{L_1})\frac{d}{d\underline{t}}\underline{W_0} + \frac{d}{d\underline{t}}\underline{W_1L_1} + \underline{L_R}\frac{d}{d\underline{t}}\underline{W_R} + \underline{V_B}\frac{d}{d\underline{t}}W_0 + \underline{L_D}\frac{d}{d\underline{t}}\underline{W_0} = ... \\ ... - \underline{W_0}\frac{\underline{W_R} - \underline{W_R}}{\underline{\rho_{in}}} - (\frac{f_0\underline{L_0}}{\underline{D_{H,0}}} + K_0)\frac{\underline{W_0}^2}{2\underline{\rho_0}} - (\frac{f_1\underline{L_1}}{\underline{D_{H,1}}} + K_1)\frac{\underline{W_1^2}}{2\underline{\rho_1}} - (\frac{f_R\underline{L_R}}{\underline{D_{H,r}}} + K_r)\frac{\underline{W_R}^2}{2\underline{\rho_R}}... \\ ... - (\frac{f_D\underline{L_D}}{\underline{D_{H,D}}} + K_D)\frac{\underline{W_0}^2}{2\underline{\rho_{in}}} - \frac{\underline{\rho_0L_0}}{N_{fr}} - \frac{\underline{\rho_1L_1}}{N_{fr}} - \frac{\underline{\rho_R}\underline{L_R}}{N_{fr}} - \frac{\underline{\rho_{in}}\underline{L_D}}{N_{fr}} \end{aligned} \tag{2.6}$$

With N_{fr} being the dimensionless Froude number, which is defined as the ratio between the flow inertia of the water and the gravitational acting force on it.

$$N_{fr} = \frac{\bar{W}^2v_{pc}^2}{gLA^2} \tag{2.7}$$

The equations will be solved using linear methods, so they must first be linearized. All time dependent variables are replaced by their steady state solution and a perturbation, denoted by a capital and a lower case letter respectively.

$$X = \bar{X} + \check{x} \tag{2.8}$$

As long as the perturbations are small, the product of two perturbations and a perturbation multiplied by the time derivative of a perturbation can be neglected.

$$XY = (\bar{X} + \check{x})(\bar{Y} + \check{y}) \approx \bar{X}\bar{Y} + \bar{X}\check{Y} + \bar{Y}\check{x} + \cancel{\check{x}\check{y}} \tag{2.9}$$

Applying this to all variables in equation 2.6 will yield the final momentum equation solely based on the perturbations.

$$\begin{aligned}(1 + \underline{\overline{L}_1} + \underline{L_D} + \underline{V_B})\frac{\mathrm{d}}{\mathrm{d}\underline{t}}\underline{\check{w}_0} + \underline{L_1}\frac{\mathrm{d}}{\mathrm{d}\underline{t}}\underline{\check{w}_1} + \underline{L_R}\frac{\mathrm{d}}{\mathrm{d}\underline{t}}\underline{\check{w}_R} = \left(\frac{1}{2}\left(\frac{f_0\underline{\upsilon_0}}{\underline{D_H}} - \frac{f_1\underline{\overline{\upsilon}_1}}{\underline{D_H}}\right) + \frac{1}{N_{Fr}\underline{\upsilon_0}} - \frac{1}{N_{Fr}\underline{\overline{\upsilon}_1}}\right)\underline{\check{l}_1}\cdots \\ \cdots - \left(\left(\frac{f_0\underline{\overline{L}_0}}{\underline{D_H}} + K_0\right)\underline{\overline{\upsilon}_0} + \left(\frac{f_D\underline{\overline{L}_D}}{\underline{D_H}} + K_D\right)\underline{\overline{\upsilon_{in}}} - \underline{\upsilon_{in}}\right)\underline{\check{w}_0}\cdots \\ \cdots - \left(\frac{f_1\underline{\overline{L}_1}}{\underline{D_H}} + K_1\right)\underline{\overline{\upsilon}_1\check{w}_1} + \left(-\frac{1}{2}\left(\frac{f_1\underline{\overline{L}_1}}{\underline{D_H}} + K_1\right) + \frac{\underline{\overline{L}_1}}{N_{Fr}\underline{\overline{\upsilon}_R^2}}\right)\frac{C_1 N_{\Delta h} h_{pc}}{\upsilon pc}\underline{\check{h}_1}\cdots \\ \cdots - \left(\frac{f_R\underline{\overline{L}_R}}{\underline{D_H}} + K_R + \frac{\underline{\upsilon_{in}}}{\underline{\overline{\upsilon}_R}}\right)\underline{\overline{\upsilon}_R\check{w}_R} + \left(-\frac{1}{2}\left(\frac{f_R\underline{\overline{L}_R}}{\underline{D_H}} + K_R\right) + \frac{\underline{\overline{L}_R}}{N_{Fr}\underline{\overline{\upsilon}_R^2}}\right)\frac{C_1 N_{\Delta h} h_{pc}}{\upsilon pc}\underline{\check{h}_R}\end{aligned}$$

3 Method of stability investigation

The linearized equations that describe the system can be solved to find values for all perturbed variables. Once this is done, the stability of the system as well as the properties like its frequency can be determined. This chapter will cover how the solutions are found.

3.1 Matrix equation

The final equations from section 2.3 are all linear, first order differential equations. Moreover, there is an equal amount of variables and equations for both models (13 for the low heating model and 16 for the high heating model). They can thus be be written in a matrix equation.

$$A\frac{d}{dt}\vec{x} = B\vec{x} \tag{3.1}$$

Matrices A and B contain the operating values and constants and can be seen in appendix C, while $\vec{x}$ contains all the perturbed variables. The matrix equation has solutions of the form $\vec{x} = \vec{v}e^{\lambda t}$. In this solution, $\vec{v}$ contains the amplitude and phase of the initial perturbation. λ can be complex and can thus be decomposed as $\lambda = a + bi$. Since λ is in the exponent for the solution, a contains the decay ratio and b contains the frequency of the perturbation. If a is negative, the perturbation will decrease with time, making it stable. If a is positive, the perturbation will be unstable.

Substituting the proposed solution for $\vec{x}$ in equation 3.1 and dividing by $e^{\lambda}t$ gives the following:

$$A\lambda\vec{v} = B\vec{v} \tag{3.2}$$

This is a generalized eigenvalue problem, which can be solved by finding solutions to $det(B - At) = 0$. Thus the values for λ, and by extend the system's stability and frequency, are found. The solution is determined using a *Matlab* script. Chapter 4 will expand on how this is done.

3.2 Time dependent solution

When investigating the behavior of the perturbation in time, only having λ no longer suffices. Instead, the full solution for $\vec{x}$ must be determined.

As stated in the previous section, the solutions of equation 3.1 are of the form $\vec{v}e^{\lambda t}$. The general solution is a linear combination of all these solutions [18].

$$\vec{x}(t) = \sum_{i=1}^{n} c_i v_i e^{\lambda_i t} \tag{3.3}$$

All values for λ_i and v_i can be found from equation 3.2. The values of c_i can be determined using an initial value vector $\vec{x}_0$. Because at $t = 0$ the exponent of the solution equals one, the constants are

calculated as follows:

$$\begin{pmatrix} c_1 \\ c_2 \\ \vdots \\ c_n \end{pmatrix} = \begin{pmatrix} | & | & & | \\ v_1 & v_2 & \dots & v_n \\ | & | & & | \end{pmatrix}^{-1} * \vec{x}_0 \tag{3.4}$$

The matrix V contains all the eigenvectors v_i in its columns, the first column being v_1, second column being v_2 and so on. To find $\vec{x}$, all that needs to be done is filling in equation 3.3 in matrix form.

$$\vec{x}(t) = \begin{pmatrix} | & | & & | \\ v_1 & v_2 & \dots & v_n \\ | & | & & | \end{pmatrix} \begin{pmatrix} e^{\lambda_1 t} & 0 & 0 & \cdots & 0 \\ 0 & e^{\lambda_2 t} & 0 & \cdots & 0 \\ 0 & 0 & e^{\lambda_3 t} & \cdots & 0 \\ \vdots & \vdots & \vdots & \ddots & \vdots \\ 0 & 0 & 0 & \cdots & e^{\lambda_n} \end{pmatrix} \begin{pmatrix} c_1 \\ c_2 \\ \vdots \\ c_n \end{pmatrix} \tag{3.5}$$

3.3 Operating conditions

The stability maps that are to be calculated with this model utilizes two operating conditions to describe the systems parameters. One is dependent on the inlet temperature of the core, the other on the heating power. Krijger, Lippens, Zonneveld and de Vries all used the same dimensionless numbers as conditions. The first is the phase change number, a measure for the difference in enthalpy that water undergoes as it flows through the core.

$$N_{\Delta h} = \frac{Q}{\bar{W} h_{pc}} \tag{3.6}$$

The other dimensionless variable is the subcooling number indicates the inlet enthalpy of the coolant. Since it is assumed that the enthalpy always lies between 0 and h_{pc}, N_{sub} varies from 0 to 1.

$$N_{sub} = 1 - \frac{H_{in}}{h_{pc}} \tag{3.7}$$

Note that $N_{\Delta h} = N_{sub}$ lies exactly on the border of the low- and the high heating model. For these conditions $\frac{Q}{\bar{W}} = h_{pc} - h_{in}$, meaning the water leaves the core exactly at its pseudo-critical enthalpy. For $N_{\Delta h} \geq N_{sub}$ water has an enthalpy difference larger than needed to become supercritical. Therefore, the high heating model holds for these conditions, while for $N_{\Delta h} \leq N_{sub}$ the low heating model does.

4 Computational Implementation

In chapters 2 and 3, the theoretical and mathematical interpretation of the reactor are explained. The results of said interpretations are acquired using a *Matlab* script. This chapter explains how the script solves all the equation mentioned and generates the results seen in chapter 6 that come from them.

4.1 Algorithm

The code used followed the same general structure as Krijger's, Lippens', Zonneveld's and de Vries' code. This layout is displayed in figure 4.1. The only differences between figure 4.1 and the figure in Zonneveld's report, which is where it was adapted from, are the introduction of a third `FOR`-loop and the creation of the frequency map. These additions are indicated by the red boxes and arrows in the figure. The extra `FOR`-loop allows for a multitude of instability maps to be generated with a single script, all for different parameters. This mostly offers convenience and is particularly useful when changing multiple parameters in one run of the code.

To give a brief overview of the code, it starts by clearing the workspace. Then all the constants and input variables which are to remain constant through the entire script are specified, including the resolution of the instability map and the steady state calculations. $N_{\Delta h}$ and N_{sub} are assigned a linear spacing of values that cover their entire range, and the variable parameters are ascribed all their values in a vector. Then, for the first value of the variable parameter, the code calculates the eigenvalues for every combination of N_{sub} and $N\Delta h$ using two `FOR`-loops. The distinction of the low- and high heating model is made using an IF loop, with the condition $N_{\Delta h} \leq N_{sub}$ meaning the low heating model is used. In the IF-loop the steady state values are calculated iteratively using a `WHILE`-loop. Once determined, these are used to calculate all flow-dependent variables.

This gives enough information to fill in the matrices seen in section 3.1. If any of eigenvalues found from solving the equation has a positive real part, a 0 is assigned to that combination of $N_{\Delta h}$ and N_{sub} to indicate it is unstable. If none of the eigenvalues are negative a 1 is assigned for that combination being stable. The imaginary part of the eigenvalue is used to calculate the frequency. This is done for all combinations of $N_{\Delta h}$ and N_{sub} , which then allows for the instability map and frequency map to be drawn. The whole process is then repeated for all values of the variable parameter, resulting in several instability maps and frequency maps.

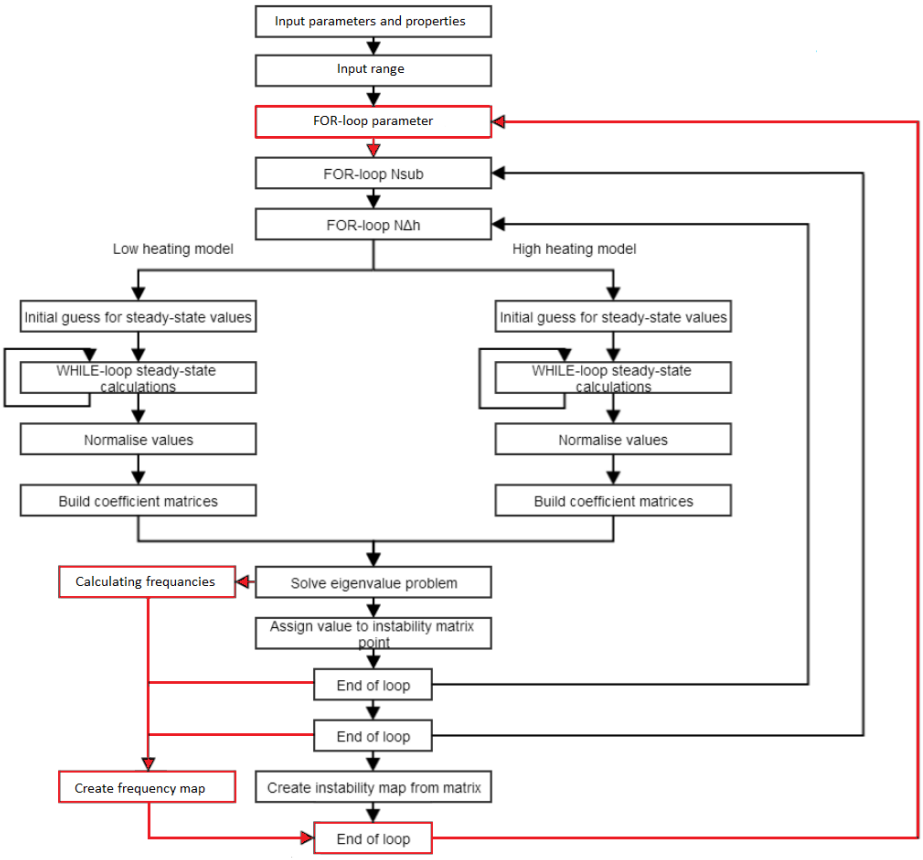

Figure 4.1: General design of the algorithm. This figure is an adaptation from Zonneveld [19]

5 Numerical experiments

With the model and computational implementation thereof explained in the previous chapters, this chapter details how everything covered so far is used to investigate the workings of the reactor. This includes three different studies. The first is a parametric study where both the length and hydraulic diameter of the riser are varied. The second is a frequency analysis on specific parts of the instability map. The third is the analysis of the time-dependent solutions of the perturbations and their impact on gravitation and friction related behavior of the system.

5.1 Parametric study

In section 1.5, it was mentioned that Krijger found that increasing the riser length decreased the stability of the system, as both regions of instability increased in size. This contradicted with earlier research done by van Bragt [16]. Van Bragt's research concerned a boiling water reactor. However, the pressure drop in a BWR is quite similar to that of the HPLWR described by the model used by Krijger. Moreover, the instabilities in both reactors are mostly type I and II DWO in both reactors. The reactors were thus expected to show similar behavior.

Van Bragt concludes in his analysis that increasing the riser length increases the size of the unstable area on the stability map associated with type I DWO, but decreases the unstable region related to type II DWO. This would imply that increasing the riser length increases the gravitational density fluctuations relative to those caused by friction. In Krijger's analysis density fluctuations from both causes increase.

The purpose of this parametric study is to explain the difference between Krijger's and van Bragt's findings. As the difference between the studies lies in the area where instabilities are mostly caused by friction, to find the cause of the difference the friction instabilities will be analyzed.

The pressure drop due to friction can be calculated as such:

$$\Delta P_{friction} = (\frac{fL}{D_H} + K)\frac{W^2}{2\rho} \tag{5.1}$$

In his research, Krijger allowed every one of these parameters to vary per node except one: the hydraulic diameter was considered constant throughout the system. Worth noting however is that D_H influences the steady state massflow $\bar{W}$, as seen in equation 2.5, which in turn influences the friction factor.

$$f = 0.316Re^{-\frac{1}{4}} \tag{5.2}$$

$$Re = \frac{\bar{W}D_H}{A\mu} \tag{5.3}$$

Changing the hydraulic diameter could thus influence the instabilities caused by friction quite significantly, although it is not directly apparent how. Keeping it constant throughout the entire loop could thus prove to be too big of a simplification.

Contrary to Krijger, van Bragt assigned a separate value to the hydraulic diameter of every node in his model [16]. Expected is that the difference can be assigned to the different hydraulic diameters they choose. In reality the hydraulic diameter of the riser is significantly bigger than in the rest of the system. A large hydraulic diameter increases the volume : surface area ratio, which in turn increases the gravity : friction ratio. Although it is not possible to give the influence precisely, it does feel intuitive to say that a large hydraulic diameter makes gravitational caused instabilities more important relative to friction caused instabilities. This would mean that increasing the length of a riser with a high hydraulic diameter would shift the instabilities toward the type I area rather than making the system less stable overall, as seen in van Bragt's thesis.

To confirm the expectation that the different approaches to the hydraulic diameter is the cause of their contradicting results, the hydraulic diameter of the riser $D_{H,R}$ will be given a separate value from the rest of the loop. The riser length L_R will be varied in the same manner as Krijger did for multiple values of $D_{H,R}$. The results of this study will be compared to both the results found by Krijger and van Bragt.

5.2 Frequency analysis

The frequencies of the system can be investigated by looking at the imaginary part of the eigenvalues. To find the frequency of a perturbation, the imaginary part of the eigenvalue with the largest real part is taken, as that eigenvalue will dominate the behavior of the perturbations. This imaginary part is then considered the frequency of the system, also known as the resonance frequency. Because time has been made dimensionless in the equations from section 2.3, the resonance frequency taken from the eigenvalue is dimensionless as well. The frequency can be calculated using the table in appendix A.

$$f = \frac{\overline{W} v_{pc}}{AL} \underline{f} \tag{5.4}$$

The value of the resonance frequency can then be assigned to the operating conditions for which the calculations were performed. Once this is done for all combinations of $N_{\Delta h}$ and N_{sub}, a frequency map can be made. The result of doing this for the reference case can be seen in figure 5.1.

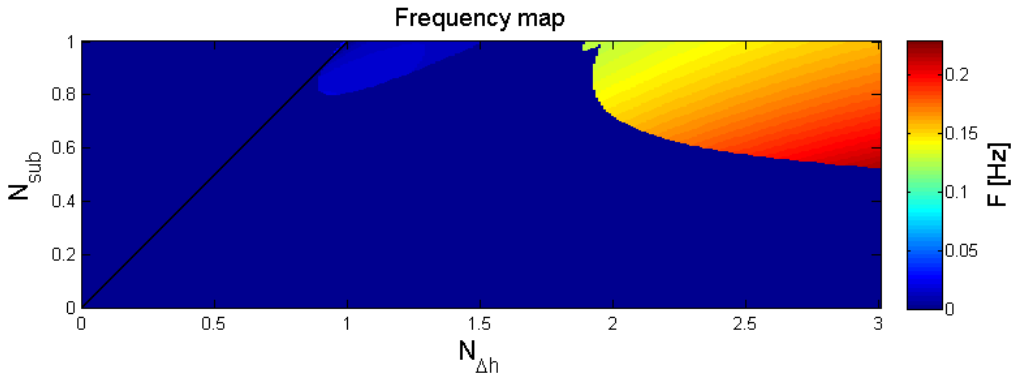

Figure 5.1: Frequency under all different operating conditions for reference case.

First thing to note is that there appears to be a higher frequency for high $N_{\Delta h}$ and for low N_{sub}. This conclusion is the same as what was found by Krijger, Lippens and Zonneveld [8][9][19]. In all their theses, this is where their analysis ended. This section will go more in depth and set up a different investigation.

In an attempt to see how the frequency of the system is determined, a closer look is taken at figure 5.1. It appears that on a straight line that goes through the origin on the frequency map, the

frequency is constant. In order to analyze this further, a dimensionless constant K is introduced for which the following holds:

$$K = \frac{N_{sub}}{N_{\Delta h}} \tag{5.5}$$

The hypothesis is that for each K, the frequency will be the same for any N_{sub} and $N_{\Delta h}$. Substituting equations 3.6 and 3.7 gives a better insight of what K actually means:

$$K = \frac{h_{pc} - h_{in}}{h_{out} - h_{in}} = 1 - \frac{L_1}{L} \tag{5.6}$$

So K is equal to the dimensionless length of the subcritical part of the core (node 0). Note that L is the total core length, which is a constant.

In order to relate K to the resonance frequency of the system, the frequency of the nodes is analyzed. The frequency of a given node is defined as the inverse of the time water is inside it. The average time water resides in a node is dependent on its length L_i and the water's speed, which will be called u_i. The speed of the water inside the node can be calculated as follows:

$$u_i = \frac{\bar{W} v_i}{A} \tag{5.7}$$

The time water remains in that node τ_i is then calculated as the length of the node over the speed of the water in it. Since equation 5.6 shows that K is effectively $\underline{L_0}$, the frequency is derived in this manner for node 0. The length can then be isolated and the expression is made dimensionless.

$$K = \frac{\tau_0 \bar{W}}{\rho_0 A L} \tag{5.8}$$

The equation can be greatly simplified by making both τ_0 and ρ_0 dimensionless. By substituting according to table A.1 most parameters fall out of the expression.

$$K = \frac{\underline{\tau_0}}{\underline{\rho_0}} \tag{5.9}$$

These are both values that can be predicted when setting the operating conditions of a reactor. If a relation between the resonance frequency and the slope K is found, substituting equation 5.9 into said relation could enable for predictions of the resonance frequency when setting the operating conditions. In the next chapter, the relation between K and the resonance frequency will be found using a fit and this derivation will be done.

5.3 Gravity and friction analysis

In section 3.2 it was explained how the time-dependent perturbations of the system could be found. Among other things, these results are useful for analyzing how behavior of the different perturbations is related. One particular application comes from the linearized momentum balance.

In the momentum balance, there are both terms clearly related to friction and ones related to gravity. Terms that include the Darcy friction factor f_i or friction coefficient K_i are friction related, while terms with the Froude Number N_{Fr} are gravitational. By taking out the friction and gravity related terms separately and summing them, two new equations are found, or four if both the low heating model and the high heating model are considered. By filling in the perturbed variables found as described in section 3.2 the temporal behavior of the system can be better understood. In particular it is useful to see which operating conditions cause the system to be mostly dictated by friction, and for which gravity is more important. The friction and gravity formula of the high heating model are displayed below.

$$F_{HHM} = \left(\frac{1}{2}\left(\frac{f_0\upsilon_0}{\underline{D_H}} - \frac{f_1\overline{\upsilon}_1}{\underline{D_H}}\right)\right)\breve{\underline{l}_1} - \left(\left(\frac{f_0\overline{\underline{L}_0}}{\underline{D_H}} + K_0\right)\overline{\upsilon}_0 + \left(\frac{f_D\overline{\underline{L}_D}}{\underline{D_H}} + K_D\right)\overline{\upsilon_{in}}\right)\breve{\underline{w}_0}\cdots$$
$$\cdots - \left(\frac{f_1\overline{\underline{L}_1}}{\underline{D_H}} + K_1\right)\overline{\upsilon}_1\breve{w}_1 + \left(-\frac{1}{2}\left(\frac{f_1\overline{\underline{L}_1}}{\underline{D_H}} + K_1\right)\right)\frac{C_1N_{\Delta h}h_{pc}}{\upsilon pc}\breve{\underline{h}_1}\cdots$$
$$\cdots - \left(\frac{f_R\overline{\underline{L}_R}}{\underline{D_H}} + K_R\right)\overline{\upsilon}_R\breve{w}_R + \left(-\frac{1}{2}\left(\frac{f_R\overline{\underline{L}_R}}{\underline{D_H}} + K_R\right)\right)\frac{C_1N_{\Delta h}h_{pc}}{\upsilon pc}\breve{\underline{h}_R} \tag{5.10}$$

$$G_{HHM} = \left(\frac{1}{N_{Fr}\underline{\upsilon_0}} - \frac{1}{N_{Fr}\underline{\overline{\upsilon}_1}}\right)\breve{\underline{l}_1} + \frac{\overline{\underline{L}_1}}{N_{Fr}\underline{\overline{\upsilon}_R^2}}\frac{C_1N_{\Delta h}h_{pc}}{\upsilon pc}\breve{\underline{h}_1} + \frac{\overline{\underline{L}_R}}{N_{Fr}\underline{\overline{\upsilon}_R^2}}\frac{C_1N_{\Delta h}h_{pc}}{\upsilon pc}\breve{\underline{h}_R} \tag{5.11}$$

Since all perturbed variables are expected to oscillate, both equations above will as well. It is thus possible to determine their amplitude and frequency. From the amplitudes a ratio of friction and gravity be determined.

$$R_{fg} = \frac{A_{friction}}{A_{gravity}} \tag{5.12}$$

R_{fr} makes it very simple to see if the system is mostly governed by gravity or friction, a high R_{fg} meaning the system is mostly ruled by friction and a low one implying its mostly ruled by gravity. Because the information is stored in one number it is also very easy to compare different operating conditions. This, among other things, gives insight in the type of instability when choosing operating conditions that make the system unstable.

The frequency of the time dependent friction and gravity perturbations is not determined using the eigenvalues as in section 5.2. Rather, since there is a calculated time signal it is now possible to determine the period T of the signal. The frequency is then found by taking the inverse of said period.

$$\underline{f} = \frac{1}{\underline{T}} \tag{5.13}$$

Note that since time has been made dimensionless, the frequency calculated this way will also be. To find the frequency in Hertz, equation 5.4 is used. The frequencies combined with the friction-gravity ratio allow for thorough examination of the instabilities. The two expected instabilities type I and type II are caused by gravity and friction respectively and have a different frequency. The first makes R_{fg} useful for analyzing the instabilities, the later makes the frequency effective.

6 Results

Chapter 5 explained the different studies that were performed. This chapter will discuss why specific choices were made in terms of chosen conditions, as well as giving the results of said studies.

6.1 Dependency on riser length and hydraulic diameter

The parametric study detailed in 5.1 has been executed with the values seen in table 6.1. The first value of the hydraulic diameter of the riser $D_{H,R}$ was chosen to be the same as in Krijger's study. This is done to ensure that the results are similar despite the fact that a different code is used and the modifications that are made to the model by Lippens and Zonneveld. For this value the hydraulic diameter of the riser is equal to that of the core and the rest of the system. In reality the riser hydraulic diameter tends to be much higher, as the core is smaller and the water flows through multiple different pipes, increasing the surface:volume ratio. Therefore the other values for $D_{H,R}$ are chosen to be bigger than the core hydraulic diameter.

Table 6.1: Values chosen for the length and hydraulic diameter of the riser

Values D_R	Values L_R
$5.6 \cdot 10^{-3}$ m	2 m
$1.0 \cdot 10^{-2}$ m	4.2 m
$5.6 \cdot 10^{-2}$ m	8 m
$5.6 \cdot 10^{-3}$ m	12 m

The riser length can really be just about anything, as there are no restrictions to it. The values of 4.2 m is chosen because this is the value of L_R in Krijger's reference case. The other values are fairly random values within a reasonable interval.

The instability border was calculated for all combinations of the riser length and hydraulic diameter of the riser from the table. To make the results easily comparable to Krijger and Bragt, the calculations with the same hydraulic diameter were all plotted in the same graph. This lead to four different graphs for every value of $D_{H,R}$ with four different instability borders for every riser length in each of them. The graphs can be seen in figure 6.1.

In the top two graphs in figure 6.1 are the ones where the hydraulic diameter of the riser is the smallest. In these graphs, a higher riser length lowers the instability border. Note that the purple line, which is the highest riser length, is the lowest line. This means a high riser lenght makes the system less stable overall, much like the case with Krijger's analysis. The top left graph, where $D_{H,R}$ is the smallest, is more extreme in this regard. The lines on the right side of the graph lie quite far apart, where in the case of the slightly higher hydraulic diameter in the top right graph the different plots are quite close to each other. In the top left graph, a third unstable area emerges in the top left graph. The origins of this region are unknown. .

The bottom two graphs show very different behavior. Here, the high riser length still has the lower border on the left half of the graph, with the purple line once again being the lowest. On the right side however, the order of the lines has been flipped, meaning a high riser length makes the system more stable for these conditions. The increase of the riser length when its hydraulic diameter is high thus leads to an increase of type I DWO instabilities, but a decrease of type II DWO. This aligns quite well with Bragt's findings. A frequency map was also made for all the different operating conditions.

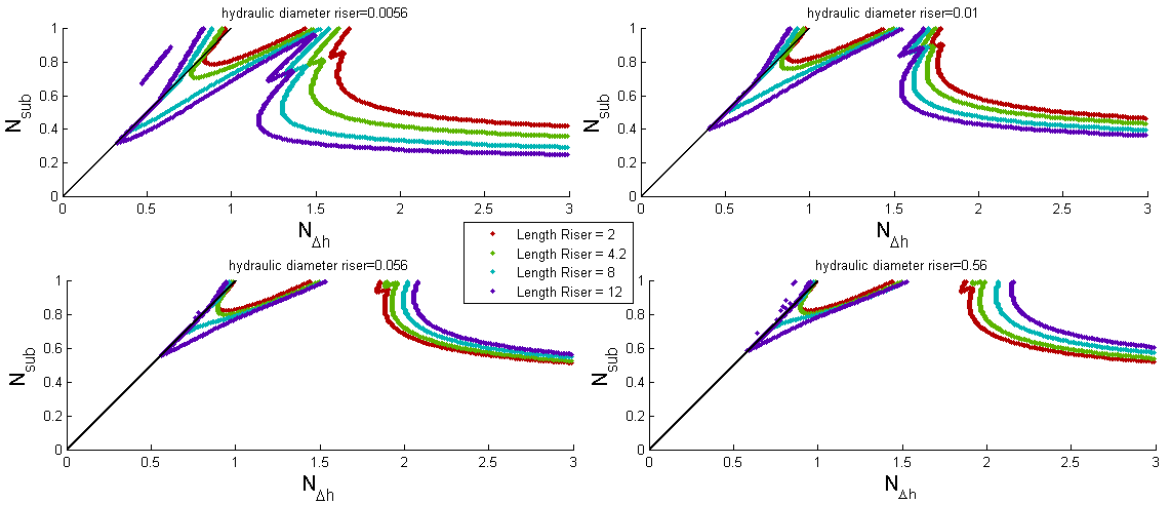

Figure 6.1: Instability lines for different riser lengths plotted in same graph, with different hydraulic diameter of the riser in every graph.

Since it is impossible to plot multiple frequency maps in a single graph, there were 16 different ones, too many to show all here.

6.2 Frequency plot

To confirm the hypothesis that the resonance frequency of the system is constant for any given K, in which case equation 5.9 holds, the resonance frequency has been calculated for several different values of K and plotted against N_{sub}. $N_{\Delta h}$ increases appropriately as N_{sub} does to stay on the lines with constant K. The plots can be seen in figure 6.2. Note that one of the plots shows an empty graph. This is because the system is empty for that value of K, meaning the code does not have any points with a resonance frequency assigned to it.

As is clear from the figure, the resonance frequency is not perfectly constant over the chosen lines. That said, the scale on the y-axis is very small, meaning only very small changes occur especially for the lower values of K. Similar plots for the mass flow and density show similar results, with the mass flow barely changing. Note that the direction of the graph changes for every value of chosen K. At low K, the frequency decreases with N_{sub} and at high K it increases.

Following these findings, for the remaining part of this section the resonance frequency will be considered constant for constant K. The next logical step is then to see how the frequency is dependent on K. To answer this, a random point on a multitude of lines associated with different K-values was chosen. The frequency on these points was calculated and that frequency was then considered the frequency for all points on that line on the instability plot. Because of the way the code is structured, the lines that do not cross into unstable regions are not assigned any frequency. These values of K can thus be recognized as the points for which frequency is zero. The found frequencies were plotted against K, which resulted in the graph seen in figure 6.3.

First thing to note is that there is a very clear difference between type I and type II Density wave oscillations in this graph. At low K, which leads to lines going through the right unstable area on the instability map, the frequencies are high. Although the frequency decreases as K increases, the decrease is not enough to explain the significant dip seen between K = 0.5 and K = 0.7. The two different types of instability do provide an explanation for this.

Something else that is noteworthy is the increase of the frequency once $K > 1$. What is also

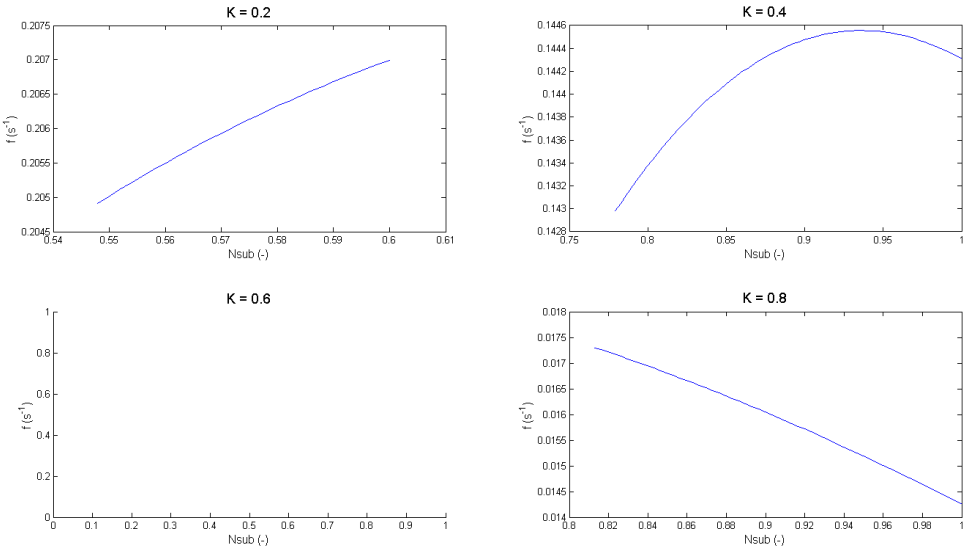

Figure 6.2: Resonance frequency against N_{sub} for along different lines in the instability plot

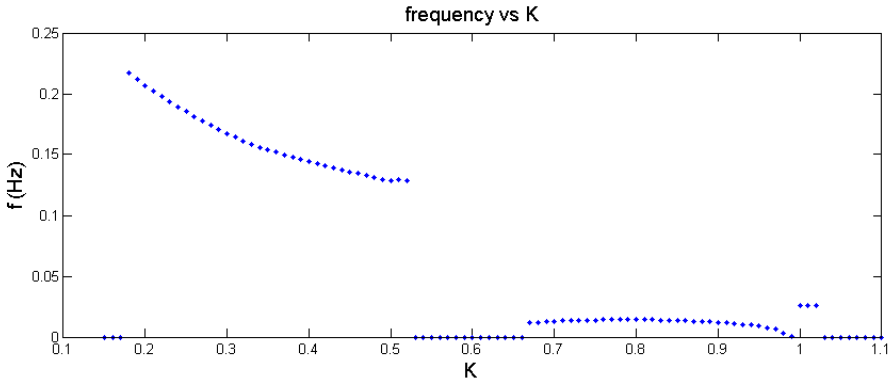

Figure 6.3: The frequency for all values of K. When f=0, the system is fully stable for that value of K

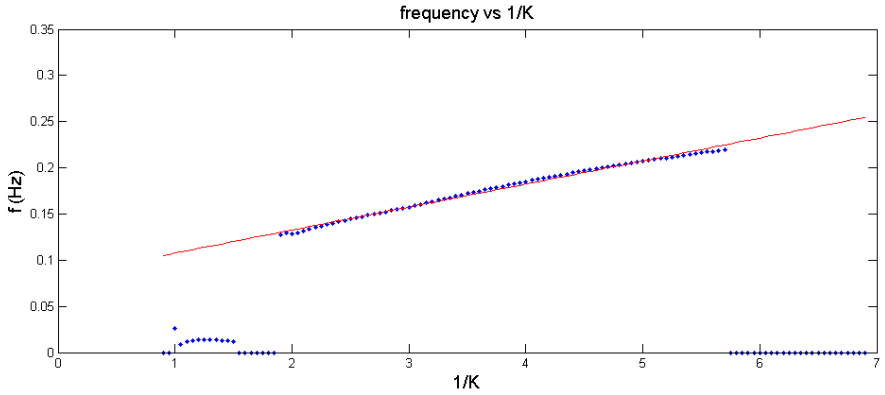

Figure 6.4: The frequency for all values of 1/K with a linear fit through the type II DWO point.

striking is that for these K, the frequency is perfectly constant. A closer look at the frequency plots shows that in this area, the frequency is indeed constant. The condition that $K > 1$ translates to the operating conditions not making the water supercritical, which means using the low heating model is applied. In section 5.2 it was shown that K influences the system by determining the length of the parts of the core where water is subcritical and supercritical. In the low heating model, the water is always subcritical, meaning $\underline{L_0} = 1$ and $\underline{L_1} = 0$. Since $\underline{L_0}$ cannot increase beyond one, the relation between $\underline{L_0}$ and K no longer holds in the low heating model. Changing K thus appears stops affecting the frequency of system altogether.

In section 5.2 it was derived that with a relation between K and the resonance frequency, the resonance frequency could be predicted given some values are known. To find this relation, the assumption is made from figure 6.3 that $f_{response}$ is linearly dependent on $\frac{1}{K}$. To test this assumption as well as to find the relation, the frequency is plotted against $\frac{1}{K}$ and using *matlab*'s curve fit tool, a linear fit is made. The resulting plot can be seen in figure 6.4

The parameters of the fit result in the following relation:

$$f_{response} = \frac{0.02491}{K} + 0.08274 \tag{6.1}$$

Taking a look back at equation 5.9, once equation 6.1 is rewritten to isolate K, there are now two expressions for K. By equating these, the final expression for the resonance frequency is found as a function of the dimensionless frequency of the subcritical part of the core and the dimensionless density of water in this core:

$$f_{response} = 0.02491 * \underline{f_0 \rho_0} + 0.08274 \tag{6.2}$$

In the high heating model, the density of the water leaving node 0 is constant as water always leaves that node when it becomes supercritical. The density of water entering the core is dependent on the operating conditions only. Since the density of water is assumed to always increase linearly, $\underline{\rho_0}$ is constant for any combination of operating conditions and can be calculated using equation 2.1. That makes the resonance frequency linearly dependent on the frequency of the subcritical part of the core.

6.3 Perturbed variables in time

The eigenvalue problem was solved as described in section 3.2, which lead to values for all the perturbed variables in time. The initial values used to calculate the constants from the linear combination to find $\vec{x}(t)$ were chosen to be 0.1 for the perturbed length of node 1, the part of the core where water is

supercritical, with others all being zero. These conditions were chosen because it is effectively seeing what happens if the power of the reactor fluctuates a bit. An increase in power will lead to the water being heated faster, making it supercritical earlier in the core, which means $\check{l}_1$ will increase. Other starting conditions were also used, but since there were no major differences in the outcomes the initial conditions will be kept constant throughout this entire section as well as the next one.

To see how the disturbance in the length of node 1 influences the system, the perturbed mass flow is plotted in both core nodes and the riser. This is done in for two different operating conditions, one leading to a stable flow and the other making the system unstable. The plots can be seen in figure 6.5 and 6.6.

As expected, under stable conditions the amplitude of the perturbation in all nodes decreases (albeit being difficult to see in figure 6.5), while for unstable conditions they all increase. Since one perturbation being unstable will impact all other perturbations, these are the only two possibilities: either all the perturbations converge or they all diverge. The plots agreed with this for all the operation conditions that were tried.

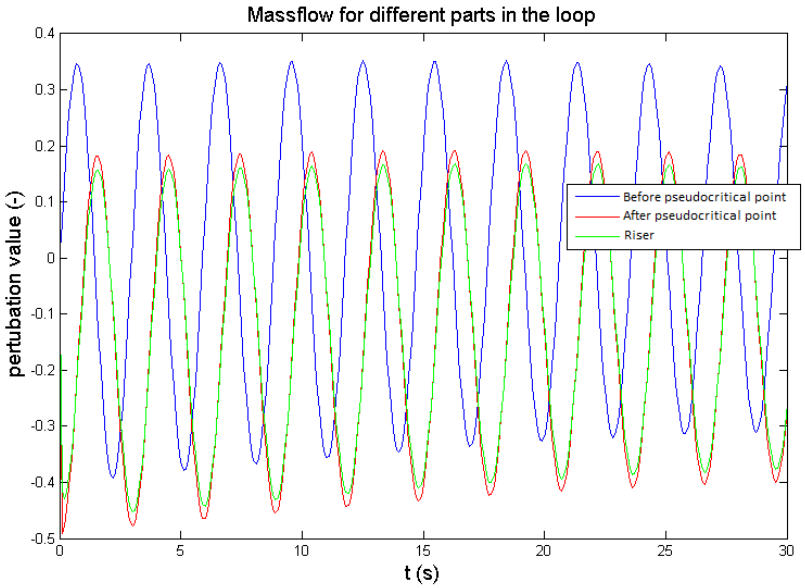

Figure 6.5: Perturbed mass flow in the two core nodes and riser for stable operating conditions $N_{\Delta h} = 1.90$ and $N_{sub} = 0.90$.

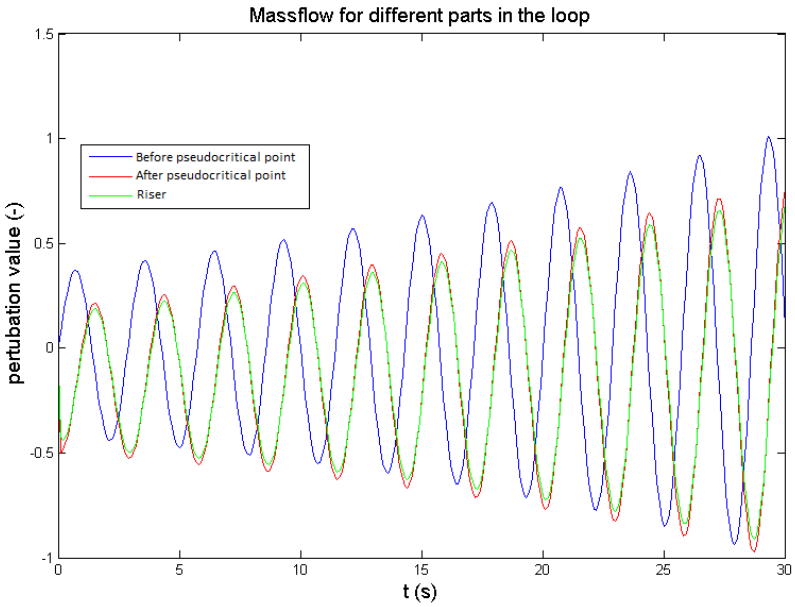

Figure 6.6: Perturbed mass flow in the two core nodes and riser for stable operating conditions $N_{\Delta h} = 1.95$ and $N_{sub} = 0.90$.

6.4 Gravity and friction in time

As described in section 5.3 an analysis was performed to see the impact that both friction and gravity had on the system. For this, four different operating conditions were chosen. Two of the chosen points were in the area where type I DWO instabilities are expected, which means that gravity is likely to be more prevalent then friction. Two points were chosen in the type II DWO area, where the opposite applies. In both the type I and type II one point was chosen for which the system was stable, and one for which it was unstable. The chosen operating points can be seen in the instability plot in figure 6.7. Note that all operating conditions fall under the high heating model, as they are to the right of the black line indicating $N_{\Delta h} = N_{sub}$.

Once the perturbed variables are calculated, they are plugged into equations 5.10 and 5.11. Then all the terms that affect the same node are taken out of said equations and summed to get the behavior of the friction terms and gravity terms in a single node. This is done for both the supercritical part of the core (node 1) and the riser.

$$F_{HHM,1} = \left(\frac{1}{2}\left(\frac{f_0\underline{\upsilon_0}}{\underline{D_H}} - \frac{f_1\overline{\upsilon}_1}{\underline{D_H}}\right)\right)\breve{\underline{l}}_1 - \left(\frac{f_1\overline{\underline{L}}_1}{\underline{D_H}} + K_1\right)\overline{\upsilon}_1\breve{w}_1 + \left(-\frac{1}{2}\left(\frac{f_1\overline{\underline{L}}_1}{\underline{D_H}} + K_1\right)\right)\frac{C_1 N_{\Delta h} h_{pc}}{\upsilon pc}\breve{\underline{h}}_1 \tag{6.3}$$

$$G_{HHM,1} = \left(\frac{1}{N_{Fr}\underline{\upsilon_0}} - \frac{1}{N_{Fr}\overline{\upsilon}_1}\right)\breve{\underline{l}}_1 + \frac{\overline{\underline{L}}_1}{N_{Fr}\overline{\upsilon}_R^2}\frac{C_1 N_{\Delta h} h_{pc}}{\upsilon pc}\breve{\underline{h}}_1 \tag{6.4}$$

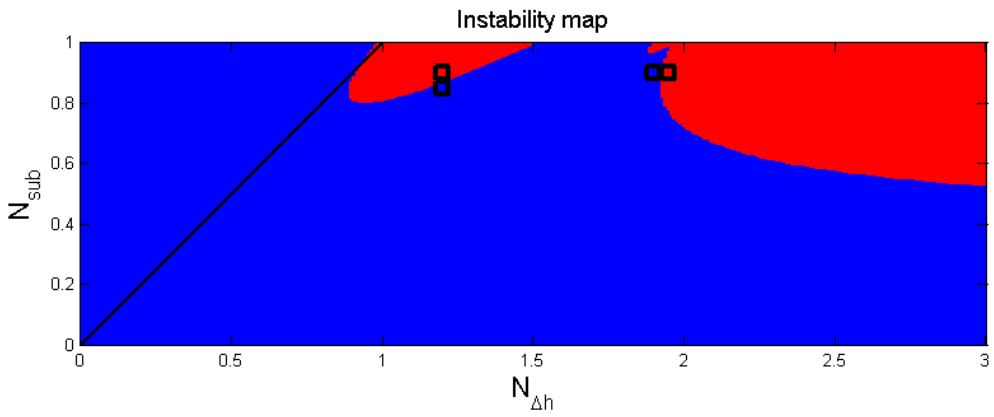

Figure 6.7: The chosen operating conditions in section 6.4, indicated by the black squares.

$$F_{HHM,R} = -\left(\frac{f_R\overline{L}_R}{\underline{D_H}} + K_R\right)\underline{\overline{v}_R\breve{w}_R} + \left(-\frac{1}{2}\left(\frac{f_R\overline{L}_R}{\underline{D_H}} + K_R\right)\right)\frac{C_1 N_{\Delta h} h_{pc}}{vpc}\underline{\breve{h}_R} \tag{6.5}$$

$$G_{HHM,R} = \frac{\overline{L}_R}{N_{Fr}\underline{\overline{v}_R^2}}\frac{C_1 N_{\Delta h} h_{pc}}{vpc}\underline{\breve{h}_R} \tag{6.6}$$

The plots that were made with the aforementioned operating conditions can be seen in figures 6.8 through 6.11. As described in section 5.3, the frequency of both the friction and gravity signal are calculated by taking the inverse of the period (formula 5.13). The ratio of friction and gravity R_{fg} was also calculated as described in formula 5.12. The ratio in node 1 is called $R_{fg,1}$ and the ratio in the riser is dubbed $R_{fg,R}$. The results of these calculations can be seen in table 6.2.

Table 6.2: Calculated values of gravity and friction plots

$N_{\Delta h}$	N_{sub}	f(Hz)	$R_{fg,1}$	$R_{fg,R}$
1.20	0.85	0.03	1.05	2.71
1.20	0.90	0.03	1.03	2.68
1.90	0.90	0.34	3.16	166
1.95	0.90	0.35	3.28	204

Note that only one frequency is displayed for every combination of $N_{\Delta h}$ and N_{sub}. This is because for constant operating conditions, the frequency of all the perturbations is the same. This results in all the formula's 6.3 through 6.6 also have the same frequency. The frequency in the table thus applies to all four signals shown in the graph belonging to those operating conditions.

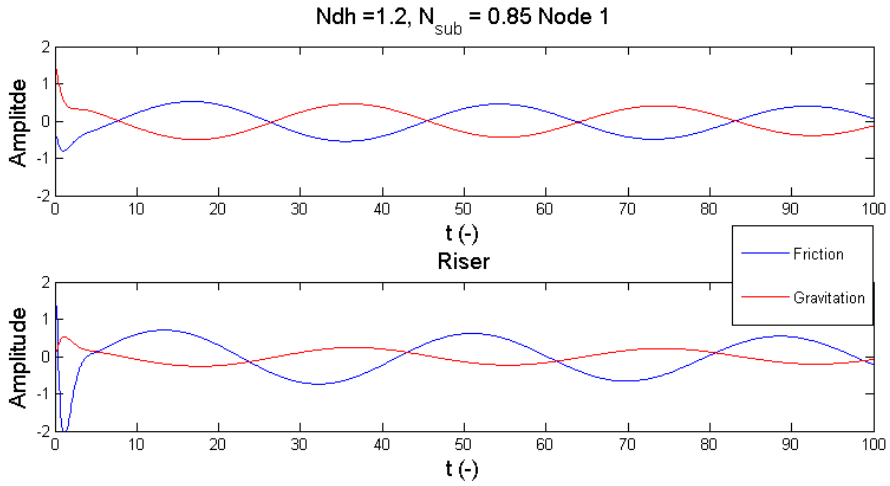

Figure 6.8: Friction and gravitation terms in the supercritical core node and riser for stable operating conditions $N_{\Delta h} = 1.20$ and $N_{sub} = 0.85$. Frequency was found to be 0.0293 Hz and R_{fg} was 1.05 in node 1 and 2.71 in node R

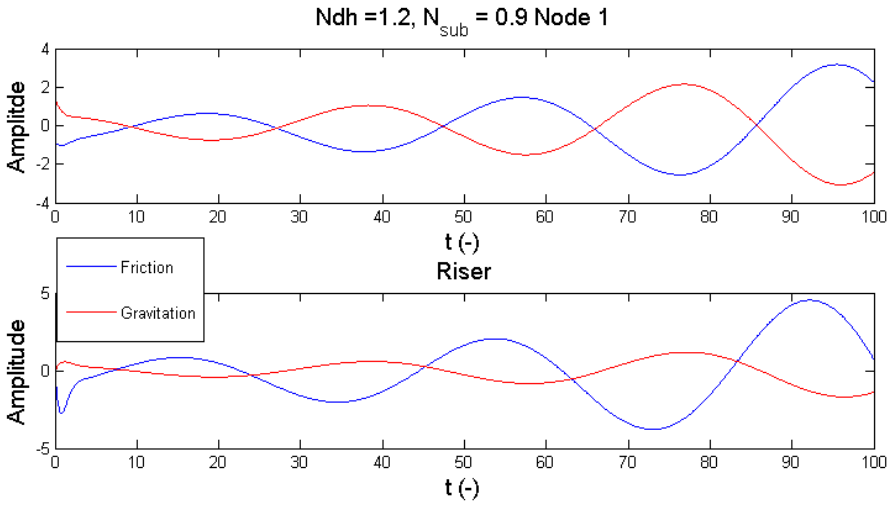

Figure 6.9: Friction and gravitation terms in the supercritical core node and riser for stable operating conditions $N_{\Delta h} = 1.20$ and $N_{sub} = 0.90$. Frequency was found to be 0.0293 Hz and R_{fg} was 1.03 in node 1 and 2.68 in node R

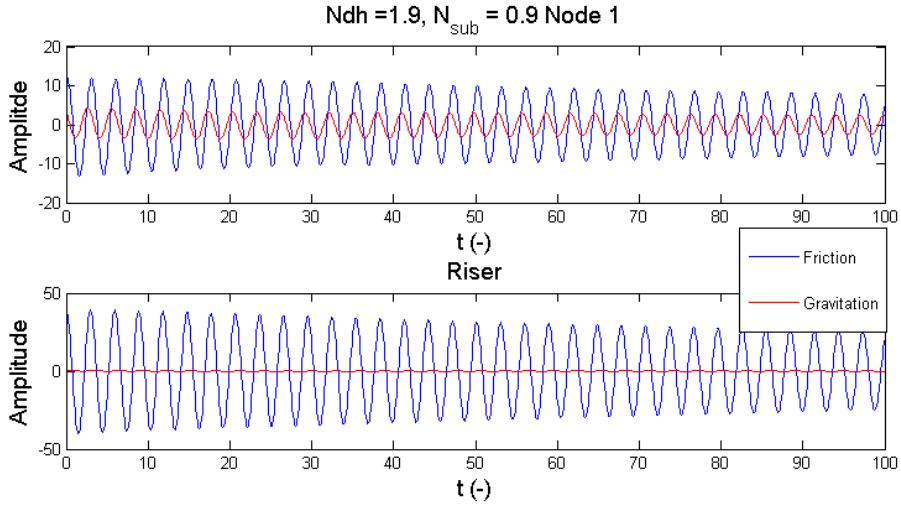

Figure 6.10: Friction and gravitation terms in the supercritical core node and riser for stable operating conditions $N_{\Delta h} = 1.90$ and $N_{sub} = 0.90$. Frequency was found to be 0.35 Hz and R_{fg} was 3.16 in node 1 and 166 in node R

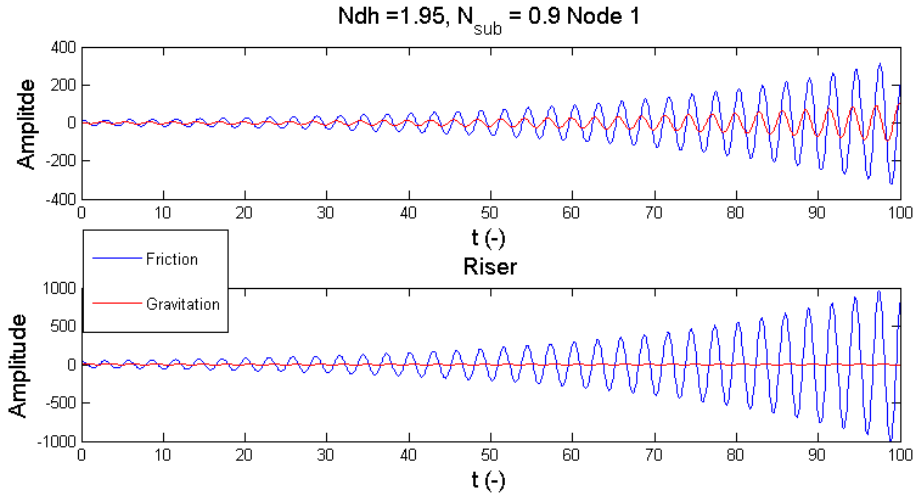

Figure 6.11: Friction and gravitation terms in the supercritical core node and riser for stable operating conditions $N_{\Delta h} = 1.95$ and $N_{sub} = 0.90$. Frequency was found to be 0.34 Hz and R_{fg} was 3.28 in node 1 and 204 in node R

Once again the signals show stable and unstable behavior for the expected operating conditions. The comparison between the different plots is most easily done with table 6.2. First thing to note is that neither the frequency nor the R_{fg} of either the riser or node 1 changes when going from stable to unstable operating conditions. The operating conditions of the first two rows lie close to each other on the instability map and so do the third and fourth row. Any major differences between the results of these rows would have to be explained by going from stable operating conditions to unstable ones. Since there are none, this appears to have no effect on frequency and R_{fg}.

There are, however, major differences between the first two rows and the last two. In terms of operating conditions, being more to the right on the instability map means $N_{\Delta h}$ increases. This increase lead to both the frequency and R_{fr} increase significantly between these conditions. The frequency increasing suggest that in the unstable regions, type II Density Wave Oscillations are most prevalent. This is further implied from the values of R_{fg} increasing, as this means friction in general has higher amplitudes in these nodes. This finding agrees very well with the expected results, as the right unstable region was expected to be type II DWO and the left one was hypothesized to be type I.

One peculiar thing to note is that the friction:gravity ratio is higher in the riser then it is in the core for all operating conditions. The hydraulic diameter of the riser was set to be a factor ten higher in these simulations. Moreover, increasing the riser length reduces the area of friction related type II instability on the instability map. It was therefore expected that it was mostly gravity that determined the behavior of this part of the loop, at least more than in the core. This means that $R_{fg,R}$ was expected to both be smaller than one and smaller than $R_{fg,1}$. The results for R_{fg} show the opposite however.

7 Conclusions and discussion

7.1 Overall conclusions

The flow instabilities inside a Supercritical-Water Reactor have been analyzed using a model developed by Krijger and augmented by Lippens and Zonneveld. The model was extended to include a time-dependent solution for all variables, as well as the ability to easily compare multiple changing parameters.

A parametric study was performed to analyze the influence of the properties of the riser. Krijger had found that with his model, increasing the riser would destabilize the system, while comparable research done in Boiling Water Reactors found that gravitational caused instabilities would increase, but frictional instabilities would decrease. The parametric study found that if the riser had a low hydraulic diameter it agreed with the results obtained by Krijger. When the hydraulic diameter increased, the behavior found by Bragt in BWR's emerged.

It was also found that on a line going through the origin of the instability plot, the resonance frequency is roughly constant. The plot of the slope and the frequency of all points on said line reinforced the assumption that the two unstable regions on the instability plots are different in origin, as the frequency drops very significantly between the two. The resonance frequency in the low heating model was found to be constant. By finding a relation between the slope of the line and the resonance frequency through fitting, an expression for the resonance frequency has been found. It was concluded to be linearly dependent on the product of the dimensionless density of the subcritical water in the core and the dimensionless frequency of node 0, which is the inverse of the time it takes for water to become supercritical once it entered the core.

The time dependent behavior of the friction and gravity elements of the momentum equation showed that in stable areas all perturbations converge, while in unstable areas they all diverge. The frequency was found to be the same for every perturbation and for every node, only depending on the operating conditions. Near the operating conditions for which type II Density Wave Oscillations were expected the frequency was of the order 0.3, while around the type I DWO's the frequency was a factor ten smaller. The amplitude of the friction perturbation proved to be larger then that of gravity under most operating conditions. In the riser friction was more significant relative to gravity then in the core node. Finally, friction was more important near type II DWO then near type I DWO.

7.2 Discussion and recommendations

The conclusion that the ratio between friction and gravity in the riser tilts towards friction more then it does in the core calls for further investigation. As mentioned in section 6.4, increasing the riser length for the used parameters improves the stability in the friction dominated area of the instability plot, while decreasing stability around the gravitational parts. Moreover, the hydraulic diameter of the riser is significantly bigger, seemingly making gravity more dominant then friction. The found results disagree with this however, something no explanation was found for in this thesis.

It should also be noted that the time plots of the perturbation rely on the linear methods. This is a fine approximation as long as the perturbations remain small, but as they get bigger the linearized

model becomes unusable. This means that the plots of perturbations in unstable regions become increasingly less accurate as they are plotted for larger time. To investigate time dependency in unstable regions for large times, another method of solving the equations must be found.

Further investigation could also be done to the frequency behavior of the system. Although the frequencies do not vary a great deal, it is not constant enough to say it truly is constant for a constant K. Especially for higher values of K, the results found in section 6.2 can be questioned. Due to the small fluctuations, results like figure 6.3, are likely to be fairly accurate, but another method of investigation might greatly improve the understanding of why certain frequencies emerge under those operating conditions. It would also likely improve the accuracy of equation 6.2

Finally, this thesis neglected looking at the Ledinegg instabilities that might occur in the system. Although they are not nearly as significant as the type I and type II DWO instabilities that this thesis does focus on, looking at them and investigating them in time might yield interesting results.

All in all, this thesis does encourage further development of the High Pressure Light Water Reactor. There are many operating conditions for which the reactor is stable and the increased understanding that comes from investigating it allows for additional control over which conditions these are.

Bibliography

[1] C T'Joen and M. Rohde. Experimental study of the coupled thermo-hydraulic-neutronic stability of a natural circulation hplwr. *Nuclear Engineering and Design*, 242:221–232, 2012.

[2] T. N. C. de Vries. Linear analysis of thermal inertia effects on the thermal-hydraulic stability of a natural circulation driven supercritical water loop, March 2016. Bachelor's thesis.

[3] K. Fischer, T. Schulenberg, and E. Laurien. Design of a supercritical water-cooled reactor with a three pass core arrangement. *Nuclear Engineering and Design*, 239(4):800–812, 2009.

[4] G Guido and J Converti and A Clausse. Density-wave oscillations in parallel channels - an analytical approach. *Nuclear Engineering and Design*, 125:121–136, 1991.

[5] GIF. Technology Roadmap Update for Generation IV Nuclear Energy Systems. `https://www.gen-4.org/gif/upload/docs/application/pdf/2014-03/gif-tru2014.pdf`, 2014.

[6] GIF. Origins of the GIF. `https://www.gen-4.org/gif/jcms/c_9334/origins`, 2016. Accessed 01-06-2016.

[7] T. O. Gómez. Stability analysis of the high performance light water reactor, 2009.

[8] D. Krijger. A linear stability analysis of a water loop driven by natural convection at supercritical conditions, July 2013. Bachelor's thesis.

[9] G. I. A. Lippens. Linear analysis of thermal inertia effects on the thermal-hydraulic stability of a natural circulation driven supercritical water loop, February 2014. Bachelor's thesis.

[10] C. P. Marcel. *Experimental and numerical stability investigations on natural circulation boiling water reactors*. PhD thesis, Delft University of Technology, October 2007.

[11] L. M. Marques, J. A. Fuinhas, and A. C. Marques. On the Global Energy Consumption and Economic Growth Nexus: a Long Time Span Analysis. *International Energy Journal*, 16:143–150, 2016.

[12] NERA. Research fields: Nuclear reactor thermal-hydraulics. `http://www.nera.rst.tudelft.nl/en/research-fields/nuclear-reactor-thermal-hydraulics/#c132314`, 2016. Accessed 01-06-2016.

[13] NIST. Thermophysical properties of fluid systems. `http://webbook.nist.gov/chemistry/fluid/`, 2011.

[14] T. Schenderling. Numerical analysis of the influence of wall thermal inertia on the stability of natural circulation driven supercritical water reactors, July 2013. Bachelor's thesis.

[15] J. Spoelstra. Numerical stability analysis of natural circulation driven supercritical water reactors. Master's thesis, Delft University of Technology, December 2012.

[16] D. D. B. van Bragt. *Analytical Modeling of Boiling Water Reactor Dynamics*. PhD thesis, Delft University of Technology, November 1998.

[17] Wikipedia. Boiling water reactor. `https://en.wikipedia.org/wiki/Boiling_water_reactor`, 2016. Accessed 01-06-2016.

[18] M.-Q. Zahn. System of first order differential equations. `https://www.unf.edu/~mzhan/chapter4.pdf`, 2007.

[19] A. Zonneveld. Linear analysis of the influence of neutronic-thermal-hydraulic coupling on the stability of a natural convection driven supercritical water loop, 2015. Bachelor's thesis.

A Dimensionless variables

In section 2.3 as well as appendix B

Table A.1: Dimensionless variables adopted from Krijger (left column) and Lippens (right column).

$\underline{\overline{L_i}} = \frac{\overline{L_i}}{L}$	Length, steady state	$\underline{T_i} = \left(\frac{\lambda_{f,pc} L}{Q}\right) T_i$	Temperature
$\underline{\breve{l}_i} = \frac{\breve{l}_i}{L}$	Length, perturbation	$\underline{\breve{\theta}_i} = \left(\frac{\lambda_{f,pc} L}{Q}\right) \breve{\theta}_i$	Temperature, perturbation
$\underline{t} = \frac{t\overline{W}\upsilon_{pc}}{AL}$	Time	$\underline{\alpha_i} \left(\frac{Q\lambda_{f,pc} L}{Q}\right) \alpha_i$	Quadratic temperature approximation coefficient
$\underline{\overline{W_i}} = \frac{\overline{W_i}}{\overline{W}} = 1$	Mass flow, steady state	$\underline{c_{p,i}} = \frac{\overline{W} c_{p,i}}{\lambda_{f,pc} L}$	Specific heat capacity
$\underline{\breve{w}_i} = \frac{\breve{w}_i}{\overline{W}}$	Mass flow, perturbation	$\underline{P_{in}} = \frac{P_{in}}{L}$	Contact perimeter between channel and wall
$\underline{\overline{H_i}} = \frac{\overline{H}_i \overline{W}}{Q}$	Specific enthalpy, steady state	$\underline{\lambda_w} = \frac{\lambda_w A}{\lambda_{f,pc} L^2}$	Wall thermal conductivity
$\underline{\breve{h}_i} = \frac{\breve{h}_i \overline{W}}{Q}$	Specific enthalpy, perturbation	$\underline{A_w} = \frac{A_w}{A}$	Wall cross-sectional area
$\underline{\overline{\rho}_i} = \overline{\rho}_i \upsilon_{pc}$	Density, steady state	$\underline{\lambda_f} = \frac{\lambda_f}{\lambda_{f,pc}}$	Coolant fluid thermal conductivity
$\underline{\breve{\rho}_i} = \breve{\rho}_i \upsilon_{pc}$	Density, perturbation	$\underline{\beta_0} = \frac{\beta_0 Q}{\lambda_{f,pc} \overline{W}}$	Coolant thermal conductivity linear approximation coefficient
$\underline{D_H} = \frac{D_H}{L}$	Hydraulic diameter	$\underline{\beta_1} = \beta_1 \frac{Q}{\overline{W}}$	Coolant thermal conductivity exponential approximation coefficient
$\underline{\overline{V}_B} = \frac{\overline{V}_B}{AL}$	Buffer volume, steady state	$\underline{\widehat{Nu_0}} = \frac{\widehat{Nu_0}}{\lambda_{f,pc}^{0.66}}$	Adjusted Nusselt number

Table A.2: Dimensionless variables adopted from Zonneveld.

$\underline{\overline{n}} = \overline{n} AL$	Neutron concentration, steady state	$\underline{\overline{C}_i} = \overline{C}_i AL$	Precursor concentration, steady state

Table A.2: (continued)

$\underline{\breve{n}} = \breve{n}AL$	Neutron concentration, perturbation	$\underline{\breve{C}_i} = \breve{C}_i AL$	Precursor concentration, perturbation
$\underline{\overline{Q}_w} = \frac{\overline{Q}_w}{Q}$	Channel wall heat flux, steady state	$\underline{\lambda_i} = \lambda_i \frac{AL}{\overline{W} v_{pc}}$	Decay constant
$\underline{\breve{q}_w} = \frac{\breve{q}_w}{Q}$	Channel wall heat flux, perturbation	$\underline{\Lambda} = \Lambda \frac{\overline{W} v_{pc}}{AL}$	Neutron generation time
$\underline{\alpha_r} = \alpha_r \rho_{pc}$	Density reactivity feedback coefficient	$\underline{\Sigma_f} = \Sigma_f L$	Macroscopic neutron cross section
$\underline{v_n} = v_n \frac{AL^2}{\overline{W} v_{pc}}$	Neutron velocity	$\underline{E_f} = E_f \frac{v_{pc}}{AL h_{pc}}$	Energy released per fission event
$\underline{\tau} = \tau \frac{\overline{W} v_{pc}}{AL}$	Fuel heat transfer time constant	$\underline{V_f} = \frac{V_f}{AL}$	Fuel volume

B Balance equations

The equations explained in section 2.3 are all derived by Krijger and expanded upon by Lippens and Zonneveld. The equations they found are all shown in this appendix.

The underlined text before the equations reference what type of balance the following equation is which node it pertains. M indicates a mass balance, E an energy balance and I the momentum balance. The node indicators, which are always the second underlined symbol, refer to the same nodes as in section 2.1, as well as in the nomenclature. Note that the momentum balance does not have a node indicator, as this balance is integrated over the entire loop.

As throughout this entire thesis, the dimensionless variant of a variable X is denoted as $\underline{X}$, its steady state value as $\bar{X}$ and a perturbation as $\check{x}$

B.1 Transport balances – low heating model

$$\underline{\text{M0}}: \quad AL\frac{\mathrm{d}}{\mathrm{d}t}\rho_0 = W_0 - W_{out} \tag{B.1}$$

$$\underline{\text{MR}}: \quad AL_R\frac{\mathrm{d}}{\mathrm{d}t}\rho_R = W_{out} - W_R \tag{B.2}$$

$$\underline{\text{MB}}: \quad \rho_{in}\frac{\mathrm{d}}{\mathrm{d}t}V_B = W_R - W_0 \tag{B.3}$$

$$\underline{\text{E0}}: \quad AL\frac{\mathrm{d}}{\mathrm{d}t}\rho_0 H_0 = W_0 H_{in} - W_{out}H_{out} + \frac{Nu_0\lambda_{f,0}}{D_H}P_{in}L(T_w - T_0) \tag{B.4}$$

$$\underline{\text{ER}}: \quad AL_R\frac{\mathrm{d}}{\mathrm{d}t}\rho_R H_R = W_{out}H_{out} - W_R H_R \tag{B.5}$$

$$\begin{aligned}\underline{\text{I}}: \quad & AL\frac{\mathrm{d}}{\mathrm{d}t}W_0 + AL_R\frac{\mathrm{d}}{\mathrm{d}t}W_R + \frac{\mathrm{d}}{\mathrm{d}t}V_B W_0 + AL_D\frac{\mathrm{d}}{\mathrm{d}t}W_0 = \cdots \\ & \cdots - \left(\frac{f_0 L}{D_H} + K_0\right)\frac{W_0^2}{2\rho_0} - \left(\frac{f_R L_R}{D_H} + K_R\right)\frac{W_R^2}{2\rho_R}\cdots \\ & \cdots - \left(\frac{f_D L_D}{D_H} + K_D\right)\frac{W_0^2}{2\rho_{in}} - A^2 g\rho_0 L - A^2 g\rho_R L_R - A^2 g\rho_{in} L_D\end{aligned} \tag{B.6}$$

$$\underline{\text{EF}}: \quad \tau\frac{\partial}{\partial t}\frac{Q_w''(t)}{\overline{Q_w''}} + \frac{Q_w''(t) - \overline{Q_w''}}{\overline{Q_w''}} = \frac{Q(t) - \overline{Q}}{\overline{Q}} \tag{B.7}$$

$$\underline{\text{Ew}}: \quad \rho_w c_{p,w} A_w L\frac{\mathrm{d}}{\mathrm{d}t}T_w = Q_w - \frac{Nu_0\lambda_f}{D_H}P_{in}L(T_w - T_0) \tag{B.8}$$

$$\underline{\text{n}}: \quad \frac{\mathrm{d}}{\mathrm{d}t}n(t) = \frac{\mathcal{R}(t) - \beta}{\Lambda}n(t) + \sum_{i=1}^{6}\lambda_i C_i(t) \tag{B.9}$$

$$\underline{\text{C}_\text{i}}: \quad \frac{\mathrm{d}}{\mathrm{d}t}C_i(t) = \frac{\beta_i}{\Lambda}n(t) - \lambda_i C_i(t), \quad \text{for } i = 1\ldots 6 \tag{B.10}$$

$$\tag{B.11}$$

B.2 Transport balances – high heating model

$$\underline{\text{M0:}} \quad A\rho_0 \frac{\mathrm{d}}{\mathrm{d}t} L_0 = W_0 - W_{pc} \tag{B.12}$$

$$\underline{\text{M1:}} \quad A \frac{\mathrm{d}}{\mathrm{d}t} \rho_1 L_1 = W_{pc} - W_1 \tag{B.13}$$

$$\underline{\text{MR:}} \quad AL_R \frac{\mathrm{d}}{\mathrm{d}t} \rho_R = W_1 - W_R \tag{B.14}$$

$$\underline{\text{MB:}} \quad \rho_{in} \frac{\mathrm{d}}{\mathrm{d}t} V_B = W_R - W_0 \tag{B.15}$$

$$\underline{\text{E0:}} \quad A\rho_0 H_0 \frac{\mathrm{d}}{\mathrm{d}t} L_0 = W_0 H_{in} - W_{pc} H_{pc} + \frac{Nu_0 \lambda_f}{D_H} P_{in} L_0 (T_w, 0 - T_0) \tag{B.16}$$

$$\underline{\text{E1:}} \quad A \frac{\mathrm{d}}{\mathrm{d}t} \rho_1 L_1 H_1 = W_{pc} H_{pc} - W_1 H_1 + \frac{Nu_1 \lambda_f}{D_H} P_{in} L_1 (T_w, 1 - T_1) \tag{B.17}$$

$$\underline{\text{ER:}} \quad AL_R \frac{\mathrm{d}}{\mathrm{d}t} \rho_R H_R = W_1 H_1 - W_R H_R \tag{B.18}$$

$$\begin{aligned} \underline{\text{I:}} \quad & A \frac{\mathrm{d}}{\mathrm{d}t} W_0 L_0 + A \frac{\mathrm{d}}{\mathrm{d}t} W_1 L_1 + AL_R \frac{\mathrm{d}}{\mathrm{d}t} W_R + \frac{\mathrm{d}}{\mathrm{d}t} V_B W_0 + AL_D \frac{\mathrm{d}}{\mathrm{d}t} W_0 = \cdots \\ & \cdots - \left(\frac{f_0 L_0}{D_H} + K_0 \right) \frac{W_0^2}{2\rho_0} - \left(\frac{f_1 L_1}{D_H} + K_1 \right) \frac{W_1^2}{2\rho_1} - \left(\frac{f_R L_R}{D_H} + K_R \right) \frac{W_R^2}{2\rho_R} \cdots \\ & \cdots - \left(\frac{f_D L_D}{D_H} + K_D \right) \frac{W_0^2}{2\rho_{in}} - A^2 g \rho_0 L_0 - A^2 g \rho_1 L_1 \cdots \\ & \cdots - A^2 g \rho_R L_R - A^2 g \rho_{in} L_D \end{aligned} \tag{B.19}$$

$$\begin{aligned} \underline{\text{Ew0:}} \quad & \rho_w c_{p,w} A_w \frac{\mathrm{d}}{\mathrm{d}t} L_0 T_{w,0} = Q_w \frac{L_0}{L} - \frac{Nu_0 \lambda_f}{D_H} P_{in} L_0 (T_{w,0} - T_0) \cdots \\ & \cdots \frac{2\lambda_w}{L} A_w (T_{w,1} - T_{w,0}) \end{aligned} \tag{B.20}$$

$$\begin{aligned} \underline{\text{Ew1:}} \quad & \rho_w c_{p,w} A_w \frac{\mathrm{d}}{\mathrm{d}t} L_1 T_{w,1} = Q_w \frac{L_1}{L} - \frac{Nu_1 \lambda_f}{D_H} P_{in} L_1 (T_{w,1} - T_1) \cdots \\ & \cdots \frac{2\lambda_w}{L} A_w (T_{w,1} - T_{w,0}) \end{aligned} \tag{B.21}$$

$$\underline{\text{n:}} \quad \frac{\mathrm{d}}{\mathrm{d}t} n(t) = \frac{\frac{L_1}{L} \mathcal{R}(t) - \beta}{\Lambda} n(t) + \sum_{i=1}^{6} \lambda_i C_i(t) \tag{B.22}$$

(B.23)

B.3 Dimensionless balances – low heating model

$$\underline{\text{M0:}} \quad \frac{\mathrm{d}}{\mathrm{d}\underline{t}}\underline{\rho_0} = \underline{W_0} - \underline{L_R}\frac{\mathrm{d}}{\mathrm{d}\underline{t}}\underline{\rho_R} - \underline{W_R} \tag{B.24}$$

$$\begin{aligned}\underline{\text{E0:}} \quad & \frac{\mathrm{d}}{\mathrm{d}\underline{t}}\underline{\rho_0 H_0} = \underline{W_0 H_{in}} - \underline{H_{out}}\left(\underline{L_R}\frac{\mathrm{d}}{\mathrm{d}\underline{t}}\underline{\rho_R} + \underline{W_R}\right)\cdots \\ & + \underline{\widehat{Nu_0}\lambda_{f0}^{0.34}}\frac{\underline{P_{in}}}{\underline{D_H}}\left(\underline{T_w} - \underline{T_{pc}} - \underline{\alpha_0}\left(\underline{H_0} - h_{pc}\right)^2\cdots\right. \\ & \left.\cdots - \frac{1}{\underline{c_{p,pc}}}\left(\underline{H_0} - h_{pc}\right)\right)\end{aligned} \tag{B.25}$$

$$\underline{\text{ER:}} \quad \underline{L_R}\frac{\mathrm{d}}{\mathrm{d}\underline{t}}\underline{\rho_R H_R} = \underline{H_{out}}\left(\underline{L_R}\frac{\mathrm{d}}{\mathrm{d}\underline{t}}\underline{\rho_R} + \underline{W_R}\right) - \underline{W_R H_R} \tag{B.26}$$

$$\begin{aligned}\underline{\text{I:}} \quad & \frac{\mathrm{d}}{\mathrm{d}\underline{t}}\underline{W_0} + \underline{L_R}\frac{\mathrm{d}}{\mathrm{d}\underline{t}}\underline{W_R} + \underline{V_B}\frac{\mathrm{d}}{\mathrm{d}\underline{t}}\underline{W_0} + \underline{L_D}\frac{\mathrm{d}}{\mathrm{d}\underline{t}}\underline{W_0} = \\ & - \underline{W_0}\frac{\underline{W_R} - \underline{W_0}}{\underline{\rho_{in}}} - \left(\frac{f_0}{\underline{D_H}} + K_0\right)\frac{\underline{W_0^2}}{2\underline{\rho_0}} - \left(\frac{f_R\underline{L_R}}{\underline{D_H}} + K_R\right)\frac{\underline{W_R^2}}{2\underline{\rho_R}}\cdots \\ & \cdots - \left(\frac{f_D\underline{L_D}}{\underline{D_H}} + K_D\right)\frac{\underline{W_0^2}}{2\underline{\rho_{in}}} - \frac{\underline{\rho_0 L_0}}{N_{Fr}} - \frac{\underline{\rho_R L_R}}{N_{Fr}} + \frac{\underline{\rho_{in} L_D}}{N_{Fr}}\end{aligned} \tag{B.27}$$

$$\begin{aligned}\underline{\text{Ew:}} \quad & \underline{\rho_w c_{p,w} A_w}\frac{\mathrm{d}}{\mathrm{d}\underline{t}}\underline{T_w} = \underline{Q_w} - \underline{\widehat{Nu_0}\lambda_{f0}^{0.34}}\frac{\underline{P_{in}}}{\underline{D_H}}\left(\underline{T_w} - \underline{T_{pc}}\cdots\right. \\ & \left.\cdots - \underline{\alpha_0}\left(\underline{H_0} - h_{pc}\right)^2 - \frac{1}{\underline{c_{p,pc}}}\left(\underline{H_0} - h_{pc}\right)\right)\end{aligned} \tag{B.28}$$

$$\underline{\text{EF:}} \quad \underline{\tau}\frac{\partial}{\partial\underline{t}}\underline{Q_w''} = \underline{\Sigma_f E_f V_f v_n n} - \underline{Q_w''} \tag{B.29}$$

$$\underline{\text{n:}} \quad \frac{\mathrm{d}}{\mathrm{d}\underline{t}}\underline{n} = \frac{\mathcal{R} - \beta}{\underline{\Lambda}}\underline{n} + \sum_{i=1}^{6}\underline{\lambda_i C_i} \tag{B.30}$$

$$\underline{\text{C}_\text{i}\text{:}} \quad \frac{\mathrm{d}}{\mathrm{d}\underline{t}}\underline{C_i} = \frac{\beta_i}{\underline{\Lambda}}\underline{n} - \underline{\lambda_i C_i} \tag{B.31}$$

B.4 Dimensionless balances – high heating model

$$\underline{\text{M0:}} \quad \underline{\rho_0}\left(\frac{\underline{H_0}}{\underline{h_{pc}}}-1\right)\frac{\mathrm{d}}{\mathrm{d}\underline{t}}\underline{L_1}=\left(1-\frac{\underline{H_{in}}}{\underline{h_{pc}}}\right)\underline{W_0}-\frac{1}{\underline{h_{pc}}}(1-\underline{L_1}) \tag{B.32}$$

$$\underline{\text{M1:}} \quad \left(\underline{\rho_1}-\frac{\underline{H_0}}{\underline{h_{pc}}}\underline{\rho_0}\right)\frac{\mathrm{d}}{\mathrm{d}\underline{t}}\underline{L_1}+\underline{L_1}\frac{\mathrm{d}}{\mathrm{d}\underline{t}}\underline{\rho_1}=\frac{\underline{H_{in}}}{\underline{h_{pc}}}\underline{W_0}+\frac{1}{\underline{h_{pc}}}(1-\underline{L_1})-\underline{W_1} \tag{B.33}$$

$$\underline{\text{MR:}} \quad \underline{L_R}\frac{\mathrm{d}}{\mathrm{d}\underline{t}}\underline{\rho_R}=\underline{W_1}-\underline{W_R} \tag{B.34}$$

$$\begin{aligned}\underline{\text{E1:}} \quad & \underline{L_1}\frac{\mathrm{d}}{\mathrm{d}\underline{t}}\underline{\rho_1 H_1}+(\underline{\rho_1 H_1}-\underline{\rho_0 H_0})\frac{\mathrm{d}}{\mathrm{d}\underline{t}}\underline{L_1}=\underline{W_0 H_{in}}-\underline{W_1 H_1}\cdots\\ & \cdots+\underline{\widehat{Nu}_0\lambda_{f0}^{0.34}}\frac{\underline{\underline{P_{in}}}(1-\underline{L_1})}{\underline{D_H}}\left(\underline{T_{w,0}}-\underline{T_{pc}}-\underline{\alpha_0}\left(\underline{H_0}-h_{pc}\right)^2\cdots\right.\\ & \left.\cdots-\frac{1}{\underline{c_{p,pc}}}\left(\underline{H_0}-h_{pc}\right)\right)\cdots\\ & \cdots+\underline{\widehat{Nu}_1\lambda_{f1}^{0.34}}\frac{\underline{\underline{P_{in}}}\underline{L_1}}{\underline{D_H}}\left(\underline{T_{w,1}}-\underline{T_{pc}}-\underline{\alpha_1}\left(\underline{H_1}-h_{pc}\right)^2\cdots\right.\\ & \left.\cdots-\frac{1}{\underline{c_{p,pc}}}\left(\underline{H_1}-h_{pc}\right)\right)\end{aligned} \tag{B.35}$$

$$\underline{\text{ER:}} \quad \underline{L_R}\frac{\mathrm{d}}{\mathrm{d}\underline{t}}\underline{\rho_R H_R}=\underline{W_1 H_1}-\underline{W_R H_R} \tag{B.36}$$

$$\begin{aligned}\underline{\text{I:}} \quad & -\underline{W_0}\frac{\mathrm{d}}{\mathrm{d}\underline{t}}\underline{L_1}+(1-\underline{L_1})\frac{\mathrm{d}}{\mathrm{d}\underline{t}}\underline{W_0}+\frac{\mathrm{d}}{\mathrm{d}\underline{t}}\underline{W_1 L_1}+\underline{L_R}\frac{\mathrm{d}}{\mathrm{d}\underline{t}}\underline{W_R}+\underline{V_B}\frac{\mathrm{d}}{\mathrm{d}\underline{t}}\underline{W_0}+\underline{L_D}\frac{\mathrm{d}}{\mathrm{d}\underline{t}}\underline{W_0}=\cdots\\ & -\underline{W_0}\frac{\underline{\underline{W_R}}-\underline{\underline{W_0}}}{\underline{\rho_{in}}}-\left(\frac{\underline{f_0}\underline{L_0}}{\underline{D_H}}+K_0\right)\frac{\underline{\underline{W_0^2}}}{2\underline{\rho_0}}-\left(\frac{\underline{f_1}\underline{L_1}}{\underline{D_H}}+K_1\right)\frac{\underline{\underline{W_1^2}}}{2\underline{\rho_1}}\cdots\\ & \cdots-\left(\frac{\underline{f_R}\underline{L_R}}{\underline{D_H}}+K_R\right)\frac{\underline{\underline{W_R^2}}}{2\underline{\rho_R}}-\left(\frac{\underline{f_D}\underline{L_D}}{\underline{D_H}}+K_D\right)\frac{\underline{\underline{W_0^2}}}{2\underline{\rho_{in}}}\cdots\\ & \cdots-\frac{\underline{\rho_0}\underline{L_0}}{\underline{\underline{N_{Fr}}}}-\frac{\underline{\rho_1}\underline{L_1}}{\underline{\underline{N_{Fr}}}}-\frac{\underline{\rho_R}\underline{L_R}}{\underline{\underline{N_{Fr}}}}+\frac{\underline{\rho_{in}}\underline{L_D}}{\underline{\underline{N_{Fr}}}}\end{aligned} \tag{B.37}$$

$$\begin{aligned}\underline{\text{Ew0:}} \quad & \underline{\rho_w c_{p,w} A_w}\left(1-\underline{L_1}\right)\frac{\mathrm{d}}{\mathrm{d}\underline{t}}\underline{T_{w,0}}-\underline{\rho_w c_{p,w} A_w T_{w,0}}\frac{\mathrm{d}}{\mathrm{d}\underline{t}}\underline{L_1}=\underline{Q_w}-\underline{L_1}\cdots\\ & \cdots-\underline{\widehat{Nu}_0\lambda_{f0}^{0.34}}\frac{\underline{\underline{P_{in}}}\left(1-L_1\right)}{\underline{D_H}}\left(\underline{T_{w,0}}-\underline{T_{pc}}-\underline{\alpha_0}\left(\underline{H_0}-h_{pc}\right)^2\cdots\right.\\ & \left.\cdots-\frac{1}{\underline{c_{p,pc}}}\left(\underline{H_0}-h_{pc}\right)\right)+2\underline{\lambda_w A_w}\left(\underline{T_{w,1}}-\underline{T_{w,0}}\right)\end{aligned} \tag{B.38}$$

$$\begin{aligned}\underline{\text{Ew1:}} \quad & \underline{\rho_w c_{p,w} A_w}\underline{L_1}\frac{\mathrm{d}}{\mathrm{d}\underline{t}}\underline{T_{w,1}}+\underline{\rho_w c_{p,w} A_w T_{w,1}}\frac{\mathrm{d}}{\mathrm{d}\underline{t}}\underline{L_1}=\underline{Q_w}+\underline{L_1}\cdots\\ & \cdots-\underline{\widehat{Nu}_1\lambda_{f1}^{0.34}}\frac{\underline{\underline{P_{in}}}\underline{L_1}}{\underline{D_H}}\left(\underline{T_{w,1}}-\underline{T_{pc}}-\underline{\alpha_1}\left(\underline{H_1}-h_{pc}\right)^2\cdots\right.\\ & \left.\cdots-\frac{1}{\underline{c_{p,pc}}}\left(\underline{H_1}-h_{pc}\right)\right)-2\underline{\lambda_w A_w}\left(\underline{T_{w,1}}-\underline{T_{w,0}}\right)\end{aligned} \tag{B.39}$$

$$\underline{\text{n:}} \quad \frac{\mathrm{d}}{\mathrm{d}\underline{t}}\underline{n}=\frac{\underline{\underline{L_1}}\mathcal{R}-\beta}{\underline{\Lambda}}\underline{n}+\sum_{i=1}^{6}\underline{\lambda_i C_i} \tag{B.40}$$

B.5 Linearised balances – low heating model

$$\underline{\text{M0:}} \quad C_1 N_{\Delta h} h_{pc} \upsilon_{pc} \left(\frac{1}{2} \frac{\mathrm{d}}{\mathrm{d}\underline{t}} \breve{h}_{\underline{out}} + \underline{L_R} \frac{\mathrm{d}}{\mathrm{d}\underline{t}} \breve{h}_{\underline{R}} \right) = \underline{\breve{w}_0} - \underline{\breve{w}_R} \tag{B.41}$$

$$\begin{aligned} \underline{\text{E0:}} \quad & \left(\frac{1}{2} \overline{\rho}_{\underline{0}} + \frac{1}{2} C_1 N_{\Delta h} h_{pc} \upsilon_{pc} \underline{\overline{H}_0} \right) \frac{\mathrm{d}}{\mathrm{d}\underline{t}} \underline{\breve{h}_{out}} + C_1 N_{\Delta h} h_{pc} \upsilon_{pc} \underline{\overline{H}_{out} L_R} \frac{\mathrm{d}}{\mathrm{d}\underline{t}} \underline{\breve{h}_R} = \\ & - \underline{\breve{w}_R \overline{H}_{out}} + \underline{\breve{w}_0 \overline{H}_{in}} + \underline{\widehat{Nu_0} \overline{\lambda}_{f0}^{0.34}} \frac{\overline{P_{in}}}{\underline{D_H}} \underline{\breve{\theta}_w} \cdots \\ & \cdots - \left(\underline{\widehat{Nu_0}} \frac{\overline{P_{in}}}{\underline{D_H}} \left(\left(\underline{\alpha_0} \left(\underline{H_0} - \underline{h_{pc}} \right) + \frac{1}{2\underline{c_{p,pc}}} \right) \underline{\overline{\lambda}_{f0}^{0.34}} \cdots \right. \right. \\ & \left. \left. \cdots - 0.17 \underline{\overline{\lambda}_{f0}^{-0.66}} \left(\underline{\overline{T}_w} - \underline{\overline{T}_0} \right) \underline{\beta_0} \right) + 1 \right) \underline{\breve{h}_{out}} \end{aligned} \tag{B.42}$$

$$\begin{aligned} \underline{\text{ER:}} \quad & \left(\underline{L_R \overline{\rho}_R} - \underline{L_R} C_1 N_{\Delta h} h_{pc} \upsilon_{pc} (\underline{\overline{H}_R} - \underline{\overline{H}_{out}}) \right) \frac{\mathrm{d}}{\mathrm{d}\underline{t}} \underline{\breve{h}_R} = \\ & \underline{\breve{h}_{out}} + \underline{\overline{H}_{out} \breve{w}_R} - \underline{\breve{h}_R} - \underline{\breve{w}_R \overline{H}_R} \end{aligned} \tag{B.43}$$

$$\begin{aligned} \underline{\text{I:}} \quad & (1 + \underline{L_D} + \underline{V_B}) \frac{\mathrm{d}}{\mathrm{d}\underline{t}} \underline{\breve{w}_0} + \underline{L_R} \frac{\mathrm{d}}{\mathrm{d}\underline{t}} \underline{\breve{w}_R} = - \left(\left(\frac{f_R \underline{L_R}}{\underline{D_H}} + K_R \right) \underline{\overline{\upsilon_R}} + \underline{\upsilon_{in}} \right) \underline{\breve{w}_R} \cdots \\ & \cdots + \frac{1}{2} C_1 N_{\Delta h} h_{pc} \upsilon_{pc} \left(\frac{1}{2} \left(\frac{f_0}{\underline{D_H}} + K_0 \right) \frac{1}{\underline{\overline{\rho}_0^2}} - \frac{1}{N_{Fr}} \right) \underline{\breve{h}_{out}} \cdots \\ & \cdots + C_1 N_{\Delta h} h_{pc} \upsilon_{pc} \left(\frac{1}{2} \left(\frac{f_R \underline{L_R}}{\underline{D_H}} + K_R \right) \frac{1}{\underline{\overline{\rho}_R^2}} - \frac{\underline{L_R}}{N_{Fr}} \right) \underline{\breve{h}_R} \cdots \\ & \cdots \left(\underline{\upsilon_{in}} - \left(\frac{f_0}{\underline{D_H}} + K_0 \right) \underline{\overline{\upsilon}_0} - \left(\frac{f_D \underline{L_D}}{\underline{D_H}} + K_D \right) \underline{\upsilon_{in}} \right) \underline{\breve{w}_0} \end{aligned} \tag{B.44}$$

$$\begin{aligned} \underline{\text{Ew:}} \quad & \underline{\rho_w c_{p,w} A_w} \frac{\mathrm{d}}{\mathrm{d}\underline{t}} \underline{\breve{\theta}_w} = \underline{\breve{q}_w} - \underline{\widehat{Nu_0} \overline{\lambda}_{f0}^{0.34}} \frac{\overline{P_{in}}}{\underline{D_H}} \underline{\breve{\theta}_w} \cdots \\ & \cdots + \frac{1}{2} \underline{\widehat{Nu_0}} \frac{\overline{P_{in}}}{\underline{D_H}} \left(\underline{\overline{\lambda}_{f0}^{0.34}} \left(2\underline{\alpha_0} \left(\underline{H_0} - \underline{h_{pc}} \right) + \frac{1}{\underline{c_{p,pc}}} \right) \cdots \right. \\ & \left. \cdots - 0.34 \underline{\overline{\lambda}_{f0}^{-0.66}} \left(\underline{\overline{T}_w} - \underline{\overline{T}_0} \right) \underline{\beta_0} \right) \underline{\breve{h}_{out}} \end{aligned} \tag{B.45}$$

$$\underline{\text{EF:}} \quad \underline{\tau} \frac{\partial}{\partial \underline{t}} \underline{\breve{q}_w} = \underline{\Sigma_f E_f V_f \upsilon_n \breve{n}} - \underline{\breve{q}_w} \tag{B.46}$$

$$\underline{\text{n:}} \quad \frac{\mathrm{d}}{\mathrm{d}\underline{t}} \underline{\breve{n}} = \frac{\underline{\alpha_r \overline{n}} C_1 N_{\Delta h} h_{pc} \upsilon_{pc} \underline{\breve{h}_0} - \beta \underline{\breve{n}}}{\underline{\Lambda}} + \sum_{i=1}^{6} \underline{\lambda_i \breve{C}_i} \tag{B.47}$$

$$\underline{\text{C}_\text{i}:} \quad \frac{\mathrm{d}}{\mathrm{d}\underline{t}} \underline{\breve{C}_i} = \frac{\underline{\beta_i}}{\underline{\Lambda}} \underline{\breve{n}} - \underline{\lambda_i \breve{C}_i} \tag{B.48}$$

(B.49)

B.6 Linearised balances – high heating model

$$\underline{\text{M0:}} \quad \underline{\rho_0}\left(\frac{\underline{\underline{H_0}}}{\underline{h_{pc}}}-1\right)\frac{\mathrm{d}}{\mathrm{d}\underline{t}}\breve{\underline{l}}_1=\left(1-\frac{\underline{\underline{H_{in}}}}{\underline{h_{pc}}}\right)\breve{\underline{w}}_0+\frac{1}{\underline{h_{pc}}}\breve{\underline{l}}_1 \tag{B.50}$$

$$\underline{\text{M1:}} \quad \left(\frac{1}{\underline{\overline{v}_1}}-\frac{\underline{\underline{H_0}}}{\underline{h_{pc}}}\underline{\rho_0}\right)\frac{\mathrm{d}}{\mathrm{d}\underline{t}}\breve{\underline{l}}_1-\frac{\underline{\underline{\overline{L}_1}}C_1N_{\Delta h}h_{pc}}{\upsilon pc\underline{\overline{v}_1^2}}\frac{\mathrm{d}}{\mathrm{d}\underline{t}}\breve{\underline{h}}_1=$$
$$\frac{\underline{\underline{H_{in}}}}{\underline{h_{pc}}}\breve{\underline{w}}_0-\frac{1}{\underline{h_{pc}}}\breve{\underline{l}}_1-\breve{\underline{w}}_1 \tag{B.51}$$

$$\underline{\text{MR:}} \quad -\frac{\underline{\underline{\overline{L}_R}}C_1N_{\Delta h}h_{pc}}{\upsilon pc\underline{\overline{v}_R^2}}\frac{\mathrm{d}}{\mathrm{d}\underline{t}}\breve{\underline{h}}_R=\breve{\underline{w}}_1-\breve{\underline{w}}_R \tag{B.52}$$

$$\underline{\text{E1:}} \quad \frac{\underline{\underline{\overline{L}_1}}}{\underline{\overline{v}_1}}\left(1-\frac{\underline{\underline{\overline{H}_1}}C_1N_{\Delta h}h_{pc}}{\upsilon pc\underline{\overline{v}_1}}\right)\frac{\mathrm{d}}{\mathrm{d}\underline{t}}\breve{\underline{h}}_1+\left(\frac{\underline{\underline{\overline{H}_1}}}{\underline{\overline{v}_1}}-\underline{H_0\rho_0}\right)\frac{\mathrm{d}}{\mathrm{d}\underline{t}}\breve{\underline{l}}_1=$$
$$\underline{H_{in}}\breve{\underline{w}}_0-\underline{\overline{H}_1}\breve{\underline{w}}_1+\underline{\widehat{Nu}_0\overline{\lambda}_{f0}^{0.34}}\frac{\underline{\underline{P_{in}\overline{L}_0}}}{\underline{D_H}}\breve{\underline{\theta}}_{w,0}\cdots$$
$$\cdots-\left(\underline{\widehat{Nu}_1}\frac{\underline{\underline{P_{in}\overline{L}_1}}}{\underline{D_H}}\left(\left(2\underline{\alpha_1}\left(\underline{\overline{H}_1}-\underline{h_{pc}}\right)+\frac{1}{\underline{c_{p,pc}}}\right)\underline{\overline{\lambda}_{f1}^{0.34}}\cdots\right.\right.$$
$$\left.\left.\cdots+0.34\ \left(\underline{\overline{T}_{w,1}}-\underline{\overline{T}_1}\right)\underline{\overline{\lambda}_{f1}^{-0.66}\beta_1\lambda_z}e^{-\beta_1\overline{H}_1}\right)+1\right)\breve{\underline{h}}_1\cdots$$
$$\cdots+\underline{\widehat{Nu}_1\overline{\lambda}_{f1}^{0.34}}\frac{\underline{\underline{P_{in}\overline{L}_1}}}{\underline{D_H}}\breve{\underline{\theta}}_{w,1}+\frac{\underline{P_{in}}}{\underline{D_H}}\left(\underline{\widehat{Nu}_1\overline{\lambda}_{f1}^{0.34}}\left(\underline{\overline{T}_{w,1}}-\underline{\overline{T}_1}\right)\cdots\right.$$
$$\left.\cdots-\underline{\widehat{Nu}_0\overline{\lambda}_{f0}^{0.34}}\left(\underline{\overline{T}_{w,0}}-\underline{\overline{T}_0}\right)\right)\breve{\underline{l}}_1 \tag{B.53}$$

$$\underline{\text{ER:}} \quad \frac{\underline{\underline{\overline{L}_R}}}{\underline{\overline{v}_R}}\left(1-\frac{\underline{\underline{\overline{H}_R}}C_1N_{\Delta h}h_{pc}}{\upsilon pc\underline{\overline{v}_R}}\right)\frac{\mathrm{d}}{\mathrm{d}\underline{t}}\breve{\underline{h}}_R=\breve{\underline{h}}_1+\underline{\overline{H}_1}\breve{\underline{w}}_1-\breve{\underline{h}}_R-\underline{\overline{H}_R}\breve{\underline{w}}_R \tag{B.54}$$

$$\underline{\text{I:}} \quad (1+\underline{\overline{L}_1}+\underline{L_D}+\underline{V_B})\frac{\mathrm{d}}{\mathrm{d}\underline{t}}\breve{\underline{w}}_0+\underline{L_1}\frac{\mathrm{d}}{\mathrm{d}\underline{t}}\breve{\underline{w}}_1+\underline{L_R}\frac{\mathrm{d}}{\mathrm{d}\underline{t}}\breve{\underline{w}}_R=$$
$$\left(\frac{1}{2}\left(\frac{f_0\underline{\upsilon_0}}{\underline{\underline{D_H}}}-\frac{f_1\underline{\overline{v}_1}}{\underline{\underline{D_H}}}\right)+\frac{1}{N_{Fr}\underline{\upsilon_0}}-\frac{1}{N_{Fr}\underline{\overline{v}_1}}\right)\breve{\underline{l}}_1\cdots$$
$$\cdots-\left(\left(\frac{f_0\underline{\overline{L}_0}}{\underline{\underline{D_H}}}+K_0\right)\underline{\overline{v}_0}+\left(\frac{f_D\underline{\overline{L}_D}}{\underline{\underline{D_H}}}+K_D\right)\underline{\overline{\upsilon_{in}}}-\underline{\upsilon_{in}}\right)\underline{\breve{w}}_0\cdots$$
$$\cdots-\left(\frac{f_1\underline{\overline{L}_1}}{\underline{\underline{D_H}}}+K_1\right)\underline{\overline{v}_1\breve{w}_1}+\left(-\frac{1}{2}\left(\frac{f_1\underline{\overline{L}_1}}{\underline{\underline{D_H}}}+K_1\right)\cdots\right.$$
$$\left.\cdots+\frac{\underline{\overline{L}_1}}{N_{Fr}\underline{\overline{v}_R^2}}\right)\frac{C_1N_{\Delta h}h_{pc}}{\upsilon pc}\breve{\underline{h}}_1\cdots$$
$$\cdots-\left(\frac{f_R\underline{\overline{L}_R}}{\underline{\underline{D_H}}}+K_R+\frac{\underline{\upsilon_{in}}}{\underline{\overline{v}_R}}\right)\underline{\overline{v}_R\breve{w}_R}+\left(-\frac{1}{2}\left(\frac{f_R\underline{\overline{L}_R}}{\underline{\underline{D_H}}}+K_R\right)\cdots\right.$$
$$\left.\cdots+\frac{\underline{\overline{L}_R}}{N_{Fr}\underline{\overline{v}_R^2}}\right)\frac{C_1N_{\Delta h}h_{pc}}{\upsilon pc}\breve{\underline{h}}_R \tag{B.55}$$

$$\underline{\text{Ew0:}} \quad \underline{\rho_wc_{p,w}A_w\overline{L}_0}\frac{\mathrm{d}}{\mathrm{d}\underline{t}}\breve{\underline{\theta}}_{w,0}-\underline{\rho_wc_{p,w}A_w\overline{T}_{w,0}}\frac{\mathrm{d}}{\mathrm{d}\underline{t}}\breve{\underline{l}}_1=$$
$$(1-\underline{L_1})\breve{\underline{q}}_w+\left(\underline{\widehat{Nu}_0\overline{\lambda}_{f0}^{0.34}}\frac{\underline{\underline{P_{in}}}}{\underline{\underline{D_H}}}\left(\underline{\overline{T}_{w,0}}-\underline{\overline{T}_0}\right)-1\right)\breve{\underline{l}}_1\cdots$$
$$\cdots-\left(\underline{\widehat{Nu}_0\overline{\lambda}_{f0}^{0.34}}\frac{\underline{\underline{P_{in}\overline{L}_0}}}{\underline{\underline{D_H}}}+2\underline{\lambda_wA_w}\right)\underline{\breve{\theta}_{w,0}}+2\underline{\lambda_wA_w}\breve{\underline{\theta}}_{w,1} \tag{B.56}$$

(B.57)

$$
\begin{aligned}
\underline{\text{Ew1:}} \qquad & \underline{\rho_w c_{p,w} A_w \overline{L_1}} \frac{\mathrm{d}}{\mathrm{d}\underline{t}} \breve{\theta}_{w,1} + \underline{\rho_w c_{p,w} A_w \overline{T}_{w,1}} \frac{\mathrm{d}}{\mathrm{d}\underline{t}} \breve{l}_{\underline{1}} = \\
& \underline{L_1 \breve{q}_w} + \left(1 - \underline{\widehat{Nu_1} \overline{\lambda}_{f1}^{0.34}} \frac{P_{in}}{\underline{D_H}} \left(\underline{\overline{T}_{w,1}} - \underline{\overline{T_1}} \right) \right) \breve{l}_{\underline{1}} \cdots \\
& \cdots + \underline{\widehat{Nu_1}} \frac{P_{in} \overline{L}_1}{\underline{D_H}} \left(\left(2\underline{\alpha_1} \left(\underline{\overline{H}_1} - \underline{h_{pc}} \right) + \frac{1}{\underline{c_{p,pc}}} \right) \underline{\overline{\lambda}_{f1}^{0.34}} \cdots \right. \\
& \cdots + 0.34 \left(\underline{\overline{T}_{w,1}} - \underline{\overline{T_1}} \right) \underline{\overline{\lambda}_{f1}^{-0.66}} \beta_1 \lambda_z e^{-\beta_1 \overline{H}_1} \Big) \breve{h}_{\underline{1}} \cdots \\
& \cdots + 2\underline{\lambda_w A_w \breve{\theta}_{w,0}} - \left(\underline{\widehat{Nu_1} \overline{\lambda}_{f1}^{0.34}} \frac{P_{in} \overline{L}_1}{\underline{D_H}} + 2\underline{\lambda_w A_w} \right) \underline{\breve{\theta}_{w,1}}
\end{aligned} \tag{B.58}
$$

$$
\underline{\text{n:}} \qquad \frac{\mathrm{d}}{\mathrm{d}\underline{t}} \breve{\underline{n}} = - \frac{C_2 N_{\Delta h} h_{pc} \underline{\alpha_r \overline{L}_1 \overline{n}}}{\upsilon_{pc} \underline{\Lambda \overline{v}_1^2}} \breve{h}_{\underline{1}} - \frac{\beta}{\underline{\Lambda}} \breve{\underline{n}} + \sum_{i=1}^{6} \underline{\lambda_i \breve{C}_i} \tag{B.59}
$$

C Matrices

The matrices discussed in section 3.1 are shown in this appendix. Due to their size they had to be split up into parts.

The rows of the matrices correspond to the different balances, while the columns correspond to the perturbations of the different variables. For the low heating model starting with the first row going down, the rows correspond with M_0, E_0, E_r, I, E_w, n, C_1 through C_6 and E_f . Starting at the left the columns correspond with $\breve{h}_{out}$, $\breve{h}_r$, $\breve{w}_0$, $\breve{w}_r$, $\breve{\theta}_w$, $\breve{n}$, $\breve{C}_1$, $\breve{C}_2$, $\breve{C}_3$,$\breve{C}_4$, $\breve{C}_5$, $\breve{C}_6$ and $\breve{q}_w$ respectively.

C.1 Low heating model

Coefficient matrix A:
Columns 1 to 5

$$\begin{pmatrix}
\frac{1}{2}C_1N_{\Delta h}h_{pc}\upsilon_{pc} & C_1N_{\Delta h}h_{pc}\upsilon_{pc}\underline{L_R} & 0 & 0 & 0 \\
\frac{1}{2}(C_1N_{\Delta h}h_{pc}\upsilon_{pc}\underline{\overline{H}_0} + \underline{\rho_0} & C_1N_{\Delta h}h_{pc}\upsilon_{pc}\underline{\overline{H}_{out}L_R} & 0 & 0 & 0 \\
0 & \underline{L_R\overline{\rho}_R} + \underline{L_R}C_1N_{\Delta h}h_{pc}\upsilon_{pc}(\underline{\overline{H}_R} - \underline{\overline{H}_{out}}) & 0 & 0 & 0 \\
0 & 0 & 1 + \underline{L_D} + \underline{\overline{V}_B} & \underline{L_R} & 0 \\
0 & 0 & 0 & 0 & \underline{\rho_w c_{p,w} A_w} \\
0 & \dots & & & 0 \\
\vdots & \ddots & & & \vdots \\
0 & \dots & & & 0
\end{pmatrix}$$

Colums 6 to 13

$$\begin{pmatrix}
0 & & \dots & & 0 \\
0 & & & & \\
0 & & \ddots & & \vdots \\
0 & & & & \\
0 & & \dots & & 0 \\
1 & 0 & 0 & 0 & 0 & 0 & 0 & 0 \\
0 & 1 & 0 & 0 & 0 & 0 & 0 & 0 \\
0 & 0 & 1 & 0 & 0 & 0 & 0 & 0 \\
0 & 0 & 0 & 1 & 0 & 0 & 0 & 0 \\
0 & 0 & 0 & 0 & 1 & 0 & 0 & 0 \\
0 & 0 & 0 & 0 & 0 & 1 & 0 & 0 \\
0 & 0 & 0 & 0 & 0 & 0 & 1 & 0 \\
0 & 0 & 0 & 0 & 0 & 0 & 0 & \underline{\tau}
\end{pmatrix}$$

COEFFICIENT MATRIX B:
Column 1

$$\begin{pmatrix} 0 \\ -\left(\underline{\widehat{Nu_0}}\frac{P_{in}}{\overline{\underline{D_H}}}\left(\left(\underline{\alpha_0}\left(\underline{H_0}-\underline{h_{pc}}\right)+\frac{1}{2\underline{c_{p,pc}}}\right)\underline{\overline{\lambda}_{f0}^{0.34}}-0.17\underline{\overline{\lambda}_{f0}^{-0.66}}\left(\overline{\underline{T}}_w-\overline{\underline{T}}_0\right)\underline{\beta_0}\right)+1\right) \\ 1 \\ \frac{1}{2}C_1N_{\Delta h}h_{pc}\upsilon_{pc}\left(\frac{1}{2}\left(\frac{f_0}{\underline{D_H}}+K_0\right)\frac{1}{\overline{\underline{\rho_0^2}}}-\frac{1}{N_{Fr}}\right) \\ \frac{1}{2}\underline{\widehat{Nu_0}}\frac{P_{in}}{\overline{\underline{D_H}}}\left(\underline{\overline{\lambda}_{f0}^{0.34}}\left(2\underline{\alpha_0}\left(\underline{H_0}-\underline{h_{pc}}\right)+\frac{1}{\underline{c_{p,pc}}}\right)-0.34\underline{\overline{\lambda}_{f0}^{-0.66}}\left(\overline{\underline{T}}_w-\overline{\underline{T}}_0\right)\underline{\beta_0}\right) \\ \frac{C_1N_{\Delta h}h_{pc}\upsilon_{pc}\underline{\alpha_r}\overline{\underline{n}}}{2\underline{\Lambda}} \\ 0 \\ 0 \\ 0 \\ 0 \\ 0 \\ 0 \\ 0 \end{pmatrix}$$

Columns 2, 3

$$\begin{pmatrix} 0 & 1 \\ 0 & \overline{\underline{H}_{in}} \\ -1 & 0 \\ \frac{1}{2}C_1N_{\Delta h}h_{pc}\upsilon_{pc}\left(\frac{1}{2}\left(\frac{f_R\underline{L_R}}{\underline{D_H}}+K_R\right)\frac{1}{\overline{\underline{\rho_R^2}}}-\frac{\underline{L_R}}{\overline{\underline{N_{Fr}}}}\right) & \left(\underline{\upsilon_{in}}\left(\frac{f_0}{\underline{D_H}}+K_0\right)\overline{\underline{\upsilon_0}}-\left(\frac{f_D\underline{L_D}}{\underline{D_H}}+K_D\right)\underline{\upsilon_{in}}\right) \\ 0 & 0 \\ 0 & 0 \\ 0 & 0 \\ 0 & 0 \\ 0 & 0 \\ 0 & 0 \\ 0 & 0 \\ 0 & 0 \\ 0 & 0 \\ 0 & 0 \end{pmatrix}$$

Columns 4, 5, 6

$$\begin{pmatrix} -1 & 0 & 0 \\ -\overline{H}_{out} & \widehat{Nu_0}\overline{\lambda}_{f0}^{-0.34}\frac{P_{in}}{\overline{D_H}} & 0 \\ \overline{H}_{out} - \overline{H}_R & 0 & 0 \\ -\left(\left(\frac{f_R L_R}{\overline{D_H}} + K_R\right)\overline{\upsilon_R} + \upsilon_{in}\right) & 0 & 0 \\ 0 & -\widehat{Nu_0}\overline{\lambda}_{f0}^{-0.34}\frac{P_{in}}{\overline{D_H}} & 0 \\ 0 & 0 & -\frac{\beta}{\Lambda} \\ 0 & 0 & \frac{\beta_1}{\Lambda} \\ 0 & 0 & \frac{\beta_2}{\Lambda} \\ 0 & 0 & \frac{\beta_3}{\Lambda} \\ 0 & 0 & \frac{\beta_4}{\Lambda} \\ 0 & 0 & \frac{\beta_5}{\Lambda} \\ 0 & 0 & \frac{\beta_6}{\Lambda} \\ 0 & 0 & \Sigma_f E_f V_f \upsilon_n \end{pmatrix}$$

Columns 7 to 13

$$\begin{pmatrix} 0 & & & \cdots & & & 0 \\ 0 & & & & & & \\ 0 & & & \ddots & & & \vdots \\ 0 & & & & & & 0 \\ 0 & & & \cdots & & 0 & 1 \\ \lambda_1 & \lambda_2 & \lambda_3 & \lambda_4 & \lambda_5 & \lambda_6 & 0 \\ -\lambda_1 & 0 & 0 & 0 & 0 & 0 & 0 \\ 0 & -\lambda_2 & 0 & 0 & 0 & 0 & 0 \\ 0 & 0 & -\lambda_3 & 0 & 0 & 0 & 0 \\ 0 & 0 & 0 & -\lambda_4 & 0 & 0 & 0 \\ 0 & 0 & 0 & 0 & -\lambda_5 & 0 & 0 \\ 0 & 0 & 0 & 0 & 0 & -\lambda_6 & 0 \\ 0 & 0 & 0 & 0 & 0 & 0 & -1 \end{pmatrix}$$

C.2 High heating model

The high heating matrices follow the same principles and the columns and rows have largely the same order as the low heating matrices, with a few additional equations and variables. The rows of the high heating matrices, again starting at the top going down, correspond with M_0, M_1, M_R, E_1, E_r, I, E_{w0}, E_{w1}, n, C_1 through C_6 and E_f. Again starting left, the columns correspond to the perturbed variables $\breve{l}_1$, $\breve{h}_1$, $\breve{h}_r$, $\breve{w}_0$, $\breve{w}_1$, $\breve{w}_r$, $\breve{\theta}_w 0$, $\breve{\theta}_w 1$, $\breve{n}$, $\breve{C}_1$, $\breve{C}_2$, $\breve{C}_3$,$\breve{C}_4$, $\breve{C}_5$, $\breve{C}_6$ and $\breve{q}_w$ respectively.

COEFFICIENT MATRIX A:

Columns 1 to 3

$$\begin{pmatrix}
\underline{\rho_0}\left(\frac{H_0}{\underline{h_{pc}}}-1\right) & 0 & 0 \\
\left(\frac{1}{\underline{v_1}}-\frac{H_0}{\underline{h_{pc}}}\underline{\rho_0}\right) & -\frac{\overline{\underline{L}_1}C_1N_{\Delta h}h_{pc}}{vpc\underline{\overline{v}_1^2}} & 0 \\
0 & 0 & -\frac{\overline{\underline{L}_R}C_1N_{\Delta h}h_{pc}}{vpc\underline{\overline{v}_R^2}} \\
\left(\frac{\overline{H}_1}{\underline{\overline{v}_1}}-\underline{H_0\rho_0}\right) & \frac{\overline{\underline{L}_1}}{\underline{\overline{v}_1}}\left(1-\frac{\overline{H}_1C_1N_{\Delta h}h_{pc}}{vpc\underline{\overline{v}_1}}\right) & 0 \\
0 & 0 & \left(\underline{L_R\overline{\rho}_R}-\underline{L_R}C_1N_{\Delta h}h_{pc}\upsilon_{pc}(\underline{\overline{H}_R}-\underline{\overline{H}_{out}})\right) \\
0 & 0 & 0 \\
-\underline{\rho_w c_{p,w}A_w\overline{T}_{w,0}} & 0 & 0 \\
\underline{\rho_w c_{p,w}A_w\overline{T}_{w,1}} & 0 & 0 \\
0 & 0 & 0 \\
\vdots & \vdots & \vdots \\
0 & 0 & 0
\end{pmatrix}$$

Columns 4 to 8

$$\begin{pmatrix}
0 & \cdots & 0 \\
0 & & \\
0 & \ddots & \vdots \\
0 & & \\
0 & \cdots & 0 \\
1-\underline{\overline{L}_1}+\underline{L_D}+\underline{\overline{V}_B} & \underline{\overline{L}_1} \quad \underline{L_R} & 0 \quad 0 \\
0 & 0 \quad 0 & \underline{\rho_w c_{p,w}A_w\overline{L_0}} \quad 0 \\
0 & 0 \quad 0 & 0 \quad \underline{\rho_w c_{p,w}A_w\overline{L_1}} \\
0 & 0 \quad 0 & 0 \quad 0 \\
\vdots & \vdots & \vdots \\
0 & 0 \quad 0 & 0 \quad 0
\end{pmatrix}$$

Colums 9 to 16

$$\begin{pmatrix}
0 & \cdots & 0 \\
0 & & \\
0 & & \\
0 & \ddots & \vdots \\
0 & & \\
0 & & \\
0 & & \\
0 & \cdots & 0 \\
1\ 0\ 0 & 0\ 0\ 0\ 0 & 0 \\
0\ 1\ 0 & 0\ 0\ 0\ 0 & 0 \\
0\ 0\ 1 & 0\ 0\ 0\ 0 & 0 \\
0\ 0\ 0 & 1\ 0\ 0\ 0 & 0 \\
0\ 0\ 0 & 0\ 1\ 0\ 0 & 0 \\
0\ 0\ 0 & 0\ 0\ 1\ 0 & 0 \\
0\ 0\ 0 & 0\ 0\ 0\ 1 & 0 \\
0\ 0\ 0 & 0\ 0\ 0\ 0 & \underline{\tau}
\end{pmatrix}$$

COEFFICIENT MATRIX B:

Column 1

$$\begin{pmatrix} \frac{1}{h_{pc}} \\ -\frac{1}{h_{pc}} \\ 0 \\ \frac{P_{in}}{D_H}\left(\widehat{Nu_1}\overline{\lambda}_{f1}^{0.34}\left(\overline{T}_{w,1}-\overline{T_1}\right)-\widehat{Nu_0}\overline{\lambda}_{f0}^{0.34}\left(\overline{T}_{w,0}-\overline{T_0}\right)\right) \\ 0 \\ \frac{1}{2}\left(\frac{f_0\upsilon_0}{D_H}-\frac{f_1\overline{v}_1}{D_H}\right)+\frac{1}{N_{Fr}\upsilon_0}-\frac{1}{N_{Fr}\overline{v}_1} \\ \frac{\widehat{Nu_0}\overline{\lambda}_{f0}^{0.34}\frac{P_{in}}{D_H}\left(\overline{T}_{w,0}-\overline{T_0}\right)-1}{1-\widehat{Nu_1}\overline{\lambda}_{f1}^{0.34}\frac{P_{in}}{D_H}\left(\overline{T}_{w,1}-\overline{T_1}\right)} \\ 0 \\ \vdots \\ 0 \end{pmatrix}$$

Column 2

$$\begin{pmatrix} 0 \\ 0 \\ 0 \\ -\left(\widehat{Nu_1}\frac{P_{in}\overline{L}_1}{D_H}\left(\left(2\alpha_1\left(\overline{H}_1-h_{pc}\right)+\frac{1}{c_{p,pc}}\right)\overline{\lambda}_{f1}^{0.34}+0.34\left(\overline{T}_{w,1}-\overline{T_1}\right)\overline{\lambda}_{f1}^{-0.66}\beta_1\lambda_z e^{-\beta_1\overline{H}_1}\right)+1\right) \\ 1 \\ \left(-\frac{1}{2}\left(\frac{f_1\overline{L}_1}{D_H}+K_1\right)+\frac{\overline{L}_1}{N_{Fr}\overline{v}_R^2}\right)\frac{C_1N_{\Delta h}h_{pc}}{\upsilon pc} \\ 0 \\ \widehat{Nu_1}\frac{P_{in}\overline{L}_1}{D_H}\left(\left(2\alpha_1\left(\overline{H}_1-h_{pc}\right)+\frac{1}{c_{p,pc}}\right)\overline{\lambda}_{f1}^{0.34}+0.34\left(\overline{T}_{w,1}-\overline{T_1}\right)\overline{\lambda}_{f1}^{-0.66}\beta_1\lambda_z e^{-\beta_1\overline{H}_1}\right) \\ -\frac{C_2N_{\Delta h}h_{pc}\alpha_r\overline{L}_1\overline{n}}{\upsilon_{pc}\Lambda\overline{v}_1^2} \\ 0 \\ \vdots \\ 0 \end{pmatrix}$$

Column 3

$$\begin{pmatrix} 0 \\ 0 \\ 0 \\ 0 \\ -1 \\ \left(-\frac{1}{2}\left(\frac{f_R\overline{L}_R}{D_H}+K_R\right)+\frac{\overline{L}_R}{N_{Fr}\overline{v}_R^2}\right)\frac{C_1N_{\Delta h}h_{pc}}{\upsilon pc} \\ 0 \\ \vdots \\ 0 \end{pmatrix}$$

Columns 4, 5

$$\begin{pmatrix} 1-\frac{H_{in}}{h_{pc}} & 0 \\ \frac{H_{in}}{h_{pc}} & -1 \\ 0 & 1 \\ H_{in} & -\overline{H}_1 \\ 0 & \overline{H}_1 \\ -\left(\left(\frac{f_0\overline{L}_0}{D_H}+K_0\right)\overline{v}_0\left(\frac{f_D\overline{L}_D}{D_H}+K_D\right)\overline{v_{in}}-v_{in}\right) & -\left(\frac{f_1\overline{L}_1}{D_H}+K_1\right)\overline{v}_1 \\ 0 & 0 \\ \vdots & \vdots \\ 0 & 0 \end{pmatrix}$$

Columns 6, 7, 8

$$\begin{pmatrix} 0 & 0 & 0 \\ 0 & 0 & 0 \\ -1 & 0 & 0 \\ 0 & \widehat{Nu_0}\overline{\lambda}_{f0}^{0.34}\frac{P_{in}\overline{L}_0}{D_H} & \widehat{Nu_1}\overline{\lambda}_{f1}^{0.34}\frac{P_{in}\overline{L}_1}{D_H} \\ -\overline{H}_R & 0 & 0 \\ -\left(\frac{f_R\overline{L}_R}{D_H}+K_R+\frac{v_{in}}{\overline{v}_R}\right)\overline{v}_R & 0 & 0 \\ 0 & -\left(\widehat{Nu_0}\overline{\lambda}_{f0}^{0.34}\frac{P_{in}\overline{L}_0}{D_H}+2\lambda_w A_w\right) & 2\lambda_w A_w \\ 0 & 2\lambda_w A_w & -\left(\widehat{Nu_1}\overline{\lambda}_{f1}^{0.34}\frac{P_{in}\overline{L}_1}{D_H}+2\lambda_w A_w\right) \\ 0 & 0 & 0 \\ \vdots & \vdots & \vdots \\ 0 & 0 & 0 \end{pmatrix}$$

Columns 9 to 16

$$\begin{pmatrix} 0 & \cdots & 0 \\ 0 & & \\ 0 & \ddots & \vdots \\ 0 & & \\ 0 & & \\ 0 & & 0 \\ 0 & \cdots & 0 \quad 1-L_1 \\ 0 & \cdots & 0 \quad L_1 \\ -\frac{\beta}{\Lambda} & \lambda_1 \quad \lambda_2 \quad \lambda_3 \quad \lambda_4 \quad \lambda_5 \quad \lambda_6 & 0 \\ \frac{\beta_1}{\Lambda} & -\lambda_1 \quad 0 \quad 0 \quad 0 \quad 0 \quad 0 & 0 \\ \frac{\beta_2}{\Lambda} & 0 \quad -\lambda_2 \quad 0 \quad 0 \quad 0 \quad 0 & 0 \\ \frac{\beta_3}{\Lambda} & 0 \quad 0 \quad -\lambda_3 \quad 0 \quad 0 \quad 0 & 0 \\ \frac{\beta_4}{\Lambda} & 0 \quad 0 \quad 0 \quad -\lambda_4 \quad 0 \quad 0 & 0 \\ \frac{\beta_5}{\Lambda} & 0 \quad 0 \quad 0 \quad 0 \quad -\lambda_5 \quad 0 & 0 \\ \frac{\beta_6}{\Lambda} & 0 \quad 0 \quad 0 \quad 0 \quad 0 \quad -\lambda_6 & 0 \\ \Sigma_f E_f V_f v_n & 0 \quad 0 \quad 0 \quad 0 \quad 0 \quad 0 & -1 \end{pmatrix}$$

D Reference case parameters

Krijger, Lippens and Zonneveld all set up a reference case for the model used in this thesis. These values are mostly all taken over by this thesis. The notable exception is the hydraulic diameter of the riser, which in this thesis is considered different from the rest of the channel. The tables below show all the parameters of the reference case

Table D.1: Design parameters for the reference case

Parameter	Value
Volume buffer vessel	10^{-2}m^3
Riser length	4.2m
Core length	4.2m
Channel hydraulic diameter	$5.6 \cdot 10^{-3}\text{m}$
Riser hydraulic diameter	$5.6 \cdot 10^{-2}\text{m}$
Channel flow area	$3.55 \cdot 10^{-5}\text{m}^2$
Wall cross-sectional area	$3.55 \cdot 10^{-5}\text{m}^2$
Fuel volume per rod	$1.48 \cdot 10^{-4}\text{m}^3$
Inlet pressure loss coefficient	1
Downcomer pressure loss coefficient	1
Riser pressure loss coefficient	20

Table D.2: Material, thermodynamic and neutronic properties for the reference case

Property	Value
Water specific enthalpy, pseudo-critical point	$2.1529 \cdot 10^6\text{J kg}^{-1}$
Water specific volume, pseudo-critical point	$3.1564 \cdot 10^{-3}\text{m}^3\text{ kg}^{-1}$
Water specific heat capacity, pseudo-critical point	$7.6444 \cdot 10^4$ J kg^{-1} K^{-1}
Dynamic viscosity of water	$4.2797 \cdot 10^{-5}$ N s m^{-2}
Fuel density	$10.96 \cdot 10^3\text{kg m}^{-3}$
Wall density	$7.850 \cdot 10^3\text{kg m}^{-3}$
Wall specific heat capacity	490 J kg^{-1} K^{-1}
Wall thermal conductivity	43 W m^{-1} K^{-1}
Fuel heat transfer time constant	6 s
Energy per fission event	$2.81 \cdot 10^{-11}\text{J}$
Fuel enrichment	4% by mass
Neutron velocity	$5.72958 \cdot 10^3$ m s^{-1}

Table D.3: Delayed neutron fractions and decay constants [19]

Table D.3: (continued)

Fractions (%)		Decay constants (s^{-1})	
β_1	0.026	λ_1	0.0127
β_2	0.1459	λ_2	0.0317
β_3	0.1288	λ_3	0.115
β_4	0.2788	λ_4	0.311
β_5	0.0877	λ_5	1.40
β_6	0.0178	λ_6	3.87